California Institute of Technology
2012 Summer Undergraduate Research Fellowship

Biomolecular rate–regulator circuits

Giulia Giordano
Università degli Studi di Udine

Mentor: **Richard M. Murray**
Co-mentor: **Elisa Franco**

September 24, 2012

Contents

Abstract **6**

1 Introduction **6**
1.1 Background and motivation . . . 6
Synthetic biology: a control–theoretic approach . . . 6
Rate regulation: what for? . . . 7
Previous literature overview . . . 9
1.2 Paper outline . . . 9

2 Artificial gene networks **11**

3 Scaling up rate–regulation circuits **13**
3.1 Possible schemes . . . 13
3.2 Scaling up negative feedback architectures . . . 14
3.2.1 Handshake connection . . . 14
3.2.2 Neighbor connection . . . 14
3.2.3 Single product . . . 15
3.2.4 Negative feedback architectures: a survey . . . 19
3.3 Scaling up positive feedback architectures . . . 19
3.3.1 Handshake connection . . . 19
3.3.2 Neighbor connection . . . 22
3.3.3 Single product . . . 22
3.3.4 Positive feedback architectures: a survey . . . 24
3.4 Negative and positive feedback: a comparison . . . 24

4 Both positive and negative feedback with two genes **26**

5 Hill function and mass action kinetics models: a comparison **31**

6 Negative feedback: a new model for a viable implementation **34**
6.1 A viable DNA strand implementation: domain level design . . . 34
6.2 A more complex model . . . 39

7 Results discussion **41**
Future research goals . . . 41

8 Methods: numerical simulations **42**

Acknowledgments **43**

References **43**

List of Figures

1 (a) The DNA double helix, composed by two long polymers of nucleotides, with backbones made of sugars and phosphate groups joined by ester bonds. Attached to each sugar is one of four types of molecules called bases: adenine (A) binds to thymine (T) and cytosine (C) to guanine (G). The two strands are anti–parallel and the sequence of the four nucleobases along the backbone encodes information. (b) An example of biomolecular circuit designed to produce oscillations. 7

2 (a) Molecular differential gear, an early Institute for Molecular Manufacturing funded project (©1997 IMM). (b) DNA box for targeted transport of molecular payloads, reproduced from [1]. 7

3 (a) Industrial assembly of electronic components to obtain a computational system: ©Arduino microcontroller. (b) Molecular assembly of biochemical components to obtain cubic RNA–based scaffolds, reproduced from [2]. 8

4 Graph representations of (a) the flux regulation problem, (b) the negative feedback flux control, (c) the positive feedback flux control. Figures reproduced from [3]. . . . 9

5 Numerical solutions to the differential equations (a) of the unregulated network, leading to a flux mismatch. (b) of the network regulated by a negative feedback. (c) of the network regulated by a positive feedback. In cases (b) and (c), the flux mismatch observably reduces. Figures reproduced from [3]. 10

6 (a) Domain representation of nucleic acids and branch migration (b) On/off state of genelets (c) RNA-mediated repression (d) RNA-mediated activation. Figure reproduced from [18]. 11

7 Possible connection schemes with n genes: (a) single product, (b) "neighbor" connection, (c) "handshake" connection. 13

8 Handshake/neighbor connection negative feedback with 3 genes: graph representation. 15

9 Handshake/neighbor connection negative feedback with 3 genes: (a) numerical ODE solutions. Handshake connection negative feedback with 4 genes: (b) numerical ODE solutions. 16

10 Handshake connection negative feedback with 3 genes: steady state values of mean concentrations and mean flow mismatches shown as a function of (a) δ and (b) α. . . 17

11 Neighbor connection negative feedback with 4 genes: (a) numerical ODE solutions, (b) steady state values of mean concentrations and mean flow mismatches shown as a function of δ. 18

12 Single product negative feedback with 3 genes: (a) numerical ODE solutions; steady state values of mean concentrations and mean flow mismatches shown as a function of (b) δ, (c) α. 20

13 Single product negative feedback with 4 genes: (a) numerical ODE solutions, (b) steady state values of mean concentrations and mean flow mismatches shown as a function of δ. 21

14 Handshake/neighbor connection positive feedback with 3 genes: graph representation. 22

15 Handshake/neighbor connection positive feedback with 3 genes: (a) numerical ODE solutions. Steady state values of mean concentrations and mean flow mismatches shown as a function of (b) δ, (c) α. 23

16 Single product positive feedback with 3 genes: (a) numerical ODE solutions; steady state values of mean concentrations and mean flow mismatches shown as a function of (b) δ, (c) α. 25
17 System with both positive and negative feedback: graph representation. 26
18 System with both positive and negative feedback. If $\alpha_{\mathrm{i,neg}} \neq 0$: numerical ODE solutions when (a) δ negative is greater than δ positive, (b) δ positive is greater than δ negative. 27
19 System with both positive and negative feedback. If $\alpha_{\mathrm{i,neg}} \neq 0$: steady state values of mean concentrations and mean flow mismatches decrease (a) if δ negative increases or (b) if δ positive decreases. 28
20 System with both positive and negative feedback. If $\alpha_{\mathrm{i,pos}} \neq 0$: numerical ODE solutions when (a) δ negative is greater than δ positive, (b) δ positive is greater than δ negative. 29
21 System with both positive and negative feedback. If $\alpha_{\mathrm{i,pos}} \neq 0$: steady state values of mean concentrations and mean flow mismatches (a) decrease if δ negative increases and (b) tend to increase if δ positive increases. 30
22 Single gene with a "load", comparison between different stoichiometric feedbacks and Hill function model for negative feedback: (a) compared numerical ODE solutions; (b) steady state value of concentrations with different loads. 32
23 Single gene with a "load", comparison between different stoichiometric feedbacks and Hill function model for negative feedback: (a) steady state value of concentrations with different values of k; (b) steady state value of concentrations with mass action kinetics models as a function of the feedback strength δ. 33
24 DNA-domain implementation of the (a) three and (b) four genes negative feedback interconnection. Complementary domains have the same color. Nicked T7 promoters are in dark gray, terminator domains in light gray. The RNA output of each genelet is designed to be complementary to its activator strand. RNA species are pairwise complementary. 34
25 Transcriptional circuit implementation of the two genes interconnection: two RNA species bind to form a product and their regulatory domains are sequestered. When either species is in excess, the feedback loops are active and therefore its regulatory domains are not covered. Figure reproduced from [3]. 35
26 Transcriptional circuit implementation of the two genes negative feedback interconnection: general reaction scheme. Complementary domains have the same color. T7 promoters are in dark gray, terminator hairpin sequences in light gray. The RNA output of each genelet is designed to be complementary to its corresponding activator strand. The two RNA species are also complementary. A) Desired self-inhibition loops. B) Undesired cross–hybridization and RNaseH mediated degradation of the RNA–template complexes. Figures reproduced from [3]. 35
27 Transcriptional circuit implementation of the three genes negative feedback interconnection: possible domain level designs with the self–inhibition domains in the first position. Complementary domains have the same color. T7 promoters are in dark gray, terminator hairpin sequences in light gray. The RNA output of each genelet is designed to be complementary to its corresponding activator strand. The RNA species are also pairwise complementary. 37

28 Transcriptional circuit implementation of the three genes negative feedback interconnection: possible domain level designs with the self–inhibition domains in the third position. Complementary domains have the same color. T7 promoters are in dark gray, terminator hairpin sequences in light gray. The RNA output of each genelet is designed to be complementary to its corresponding activator strand. The RNA species are also pairwise complementary. 38
29 Transcriptional circuit implementation of the four genes negative feedback interconnection: a couple of examples of possible domain level designs. Complementary domains have the same color. T7 promoters are in dark gray, terminator hairpin sequences in light gray. The RNA output of each genelet is designed to be complementary to its corresponding activator strand. The RNA species are also pairwise complementary. . 38
30 Transcriptional circuit implementation of the negative feedback scheme: numerical ODE solutions for the case of (a) 3 genes and (b) 4 genes. 40

Abstract **— Binding of proteins and RNA underlies cell metabolism, gene expression and self–assembly phenomena. Often such binding has to occur with specific stoichiometric ratios: therefore flux control is important to regulate production rate and concentration of biochemical species. Flux control loops for two binding species forming an output product have been implemented with *in vitro* artificial gene circuits. This research project aimed at generalizing flux regulation architectures to an arbitrary number of species. Feedback loops were designed based on negative auto–regulation (which can minimize the potentially harmful amount of molecules not used to form the product), cross–activation (which can maximize the overall output flux) and both. It was shown that transcription rate matching can be achieved through proper feedback constants; negative feedback is faster and maintains stability. The performances of feedback generated with mass action kinetics and feedback described by Hill functions were compared; stoichiometric negative feedback keeps concentrations at a lower level. We also studied a possible experimental implementation of a three and four gene network for flux matching based on negative feedback.**

1 Introduction

1.1 Background and motivation

Synthetic biology: a control–theoretic approach

The project pertains to the field of synthetic biology, an emerging and challenging area of research, which aims at designing from the bottom–up new large scale biological circuits with specific functionalities.

New biotechnologies, gene and cell therapy can improve human health and quality of life. The ability of engineering genes and cells and creating new biomolecular circuits is useful to devise innovative biotechnologies and drugs — for instance, some genes have been used as blocks to insert in a host genome, to make it provide the desired behavior: yeasts and bacteria have been engineered to produce pharmaceuticals and remedies, such as insulin. The creation of new circuits is not only useful for the purpose of practical applications: it can also offer a powerful insight into the design principles present in nature and selected by evolution, that, although it works by random tinkering, seems to converge onto a defined set of basic circuit elements [4, 5, 6].

To survive, all living organisms need to sense external stimuli and face variations in the environment [3]. Cells process information, for survival and reproduction, by means of biochemical circuits made of many species of interacting molecules. Complex structures assemble, perform elaborate biochemical tasks and vanish when their work is done: these phenomena seem to be simple, since they are so spontaneous and efficient, but it is very difficult to understand the general design principles underlying their mechanisms [4]. However, it is deeply interesting to study, analyze and model the interactions among the bricks that compose and sustain life and, once we have penetrated the basic functioning of nature, it will be easier to imitate it in order to forge new biomolecular circuits with the desired behavior.

To perform the study and the design of gene circuits, it is crucial to develop predictive models, in order to highlight the fundamental features of biological circuitry and the basic laws that rule the behavior of living matter, and quantitative methods, in order to optimally adjust their features: thus a control–theoretic approach is very powerful to assess the key properties of a biochemical dynamical system, tuning its performance and robustness [7, 3].

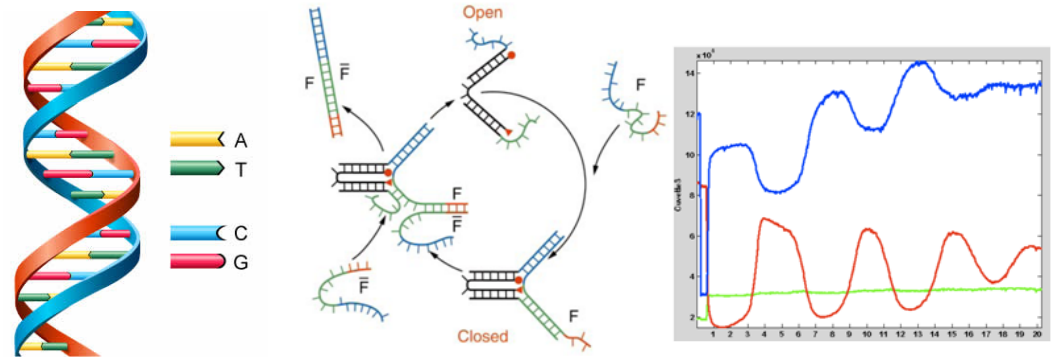

(a) (b)

Figure 1: (a) The DNA double helix, composed by two long polymers of nucleotides, with backbones made of sugars and phosphate groups joined by ester bonds. Attached to each sugar is one of four types of molecules called bases: adenine (A) binds to thymine (T) and cytosine (C) to guanine (G). The two strands are anti–parallel and the sequence of the four nucleobases along the backbone encodes information. (b) An example of biomolecular circuit designed to produce oscillations.

Rate regulation: what for?

Could we ever build complex biological systems made of simple components, as we build complex computational systems made of nanometric silicon devices? The ambition is still very far to be reached, but it is an attractive challenge [8]. Some of the basic blocks have already been built, such as clock signals [9], oscillators [10, 11, 12], elements with bistable or multistable features [13]. It is already possible to construct actual molecular machines [2] and DNA nanorobots [1].

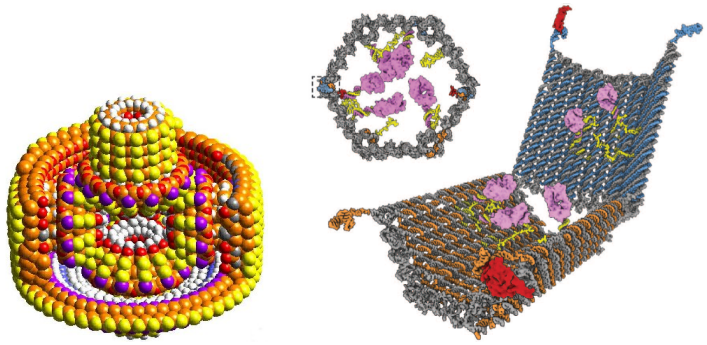

(a) (b)

Figure 2: (a) Molecular differential gear, an early Institute for Molecular Manufacturing funded project (©1997 IMM). (b) DNA box for targeted transport of molecular payloads, reproduced from [1].

Biological systems actually have a lot of features in common with those designed by human engineers. Both can reach very high levels of complexity, yet they are made of simple building blocks assembled in a modular, hierarchical design: basic functional motifs, widely diffused in nature, can be considered as the elementary building blocks of great biological systems [4, 6]; and also man–made complex systems reuse a small set of simpler components. If we are producing a complex system made

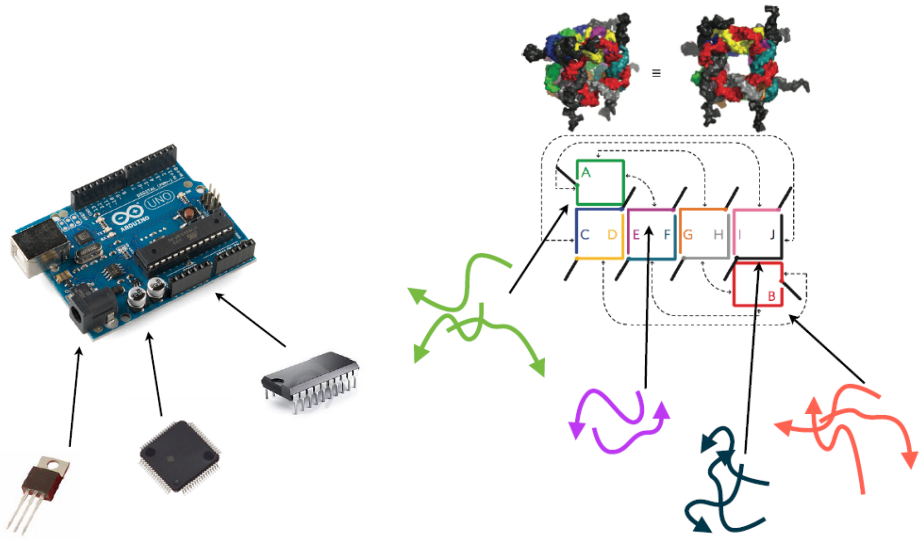

(a) (b)

Figure 3: (a) Industrial assembly of electronic components to obtain a computational system: ©Arduino microcontroller. (b) Molecular assembly of biochemical components to obtain cubic RNA–based scaffolds, reproduced from [2].

up of many smaller components, we want to produce all the components at a precise rate, in order to have exactly the needed amount of each of them. In the biomolecular case, cells heavily rely for their survival and activities on a regulated flow of nucleic acids (DNA, RNA), transcription factors, proteins and other metabolites. Binding of proteins and RNA underlies cell metabolism, gene expression and self–assembly phenomena; and often such binding has to occur with specific stoichiometric ratios. An excessive accumulation of one or more reagents is undesirable and may be dangerous; on the other side, if the production of some reagents is too slow, it becomes a bottleneck for the product flow and limits the throughput of the whole process. Flux control is thus a fundamental feature and, in a synthetic circuit, it is very important to be able to regulate and optimize molecular flow rate in order to optimize the production process. Regulatory schemes are necessary to avoid excess production of molecules unused by the cell and to increase the production of molecules highly required.

In vitro synthetic gene networks have been recently proposed in [13, 11]: the activity of artificial, short DNA genes ("genelets") is regulated by their RNA outputs, through displacement of key activating strands bound to the genes. Thus, unlike *in vivo* transcriptional control, regulation is mediated by RNA species rather than by proteins. These networks are translation free (i.e. no proteins are produced) and are built with few biochemical components (DNA, RNA, two protein species off-the-shelf, and a well defined set of buffer reagents), but can exhibit by design complex behaviors such as bistability [13, 14] and oscillations [11, 9]. Since they can generate many complex behaviors, *in vitro* transcriptional circuits are a promising toolkit to control dynamics in molecular machines [2, 1], patterns [15] and computers [16]. Thus, we need scalable flux control architectures tailored to these synthetic gene networks.

The present project is focused on a class of synthetic gene circuits, termed "rate regulators", which interact to regulate their RNA production rate. The first rate regulator circuits designed *in vitro* involve two genes, do not correspond to any biological circuit existing in nature and are

described in [17, 8, 3].

Previous literature overview

The simplest case of flux regulation is given by two reagents that bind one to one to form a product. The aim is to equate their flow (or, more in general, to regulate the different flows depending on the stoichiometric ratios of the reaction that has to occur) through the design of feedback loops. As a model problem, consider two reactants, R_1 and R_2 (produced at rates β_1 and β_2 by the genes T_1 and T_2, respectively), that bind with one to one stoichiometry to form an output product P [3]. If the two flows are not matched, the reagent with the higher flux accumulates, creating a potentially harmful excess, and the flow of product is limited by the lower reagent flux. We would like thus to reduce the flux mismatch, namely the difference in absolute value between the two production rates. To equate the two production rates, regulatory schemes are necessary and two different designs have been proposed in literature up to now: the first is based on negative feedback (self–repression [17]), the second on positive feedback (cross–activation [8]). The problem considered and the two designs devised in previous literature are shown in Fig. 4. The first design [17, 3] performs self–repression of the species in excess: when either species senses an excess of its product, it down–regulates its own production rate. The second design [8, 3] performs cross–activation: if one of the reagents is in excess, it will increase the production rate of the other reagent. Since both transcripts have this self–repression or cross–activation feature, at steady state their production rates will be equal. The differential equations describing the dynamics of the species concentrations in the three cases can be gathered from chemical reactions through mass action kinetics and the solution trajectories, obtained via numerical simulations, are shown in Fig. 5 for a particular set of parameter values: both negative and positive feedback can balance the quantity of reactants produced. As these gene circuits have been built *in vitro*, the numerical results have been confirmed by experiments.

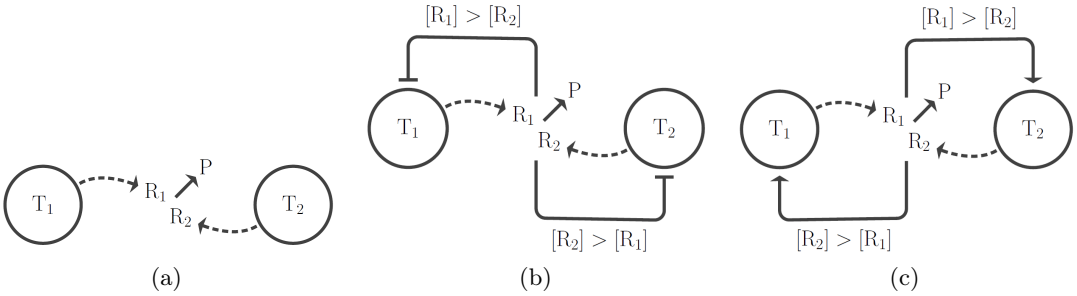

Figure 4: Graph representations of (a) the flux regulation problem, (b) the negative feedback flux control, (c) the positive feedback flux control. Figures reproduced from [3].

1.2 Paper outline

The goal of the project was to develop new and more general models that describe rate–regulation circuits, to extend these patterns to more than two genes, by using positive or negative feedback, to examine the sensitivity to parameter variation and the robustness of the models and to make comparisons between different scenarios and performances.

The existing models and experimental implementations of synthetic rate regulatory circuits are limited to connecting only two genes, but, to make these schemes useful for large scale systems, we needed to be able to describe and monitor situations in which genes and metabolites are interacting in greater number. Besides generalizing the models, we wanted to discover what kind of feedback

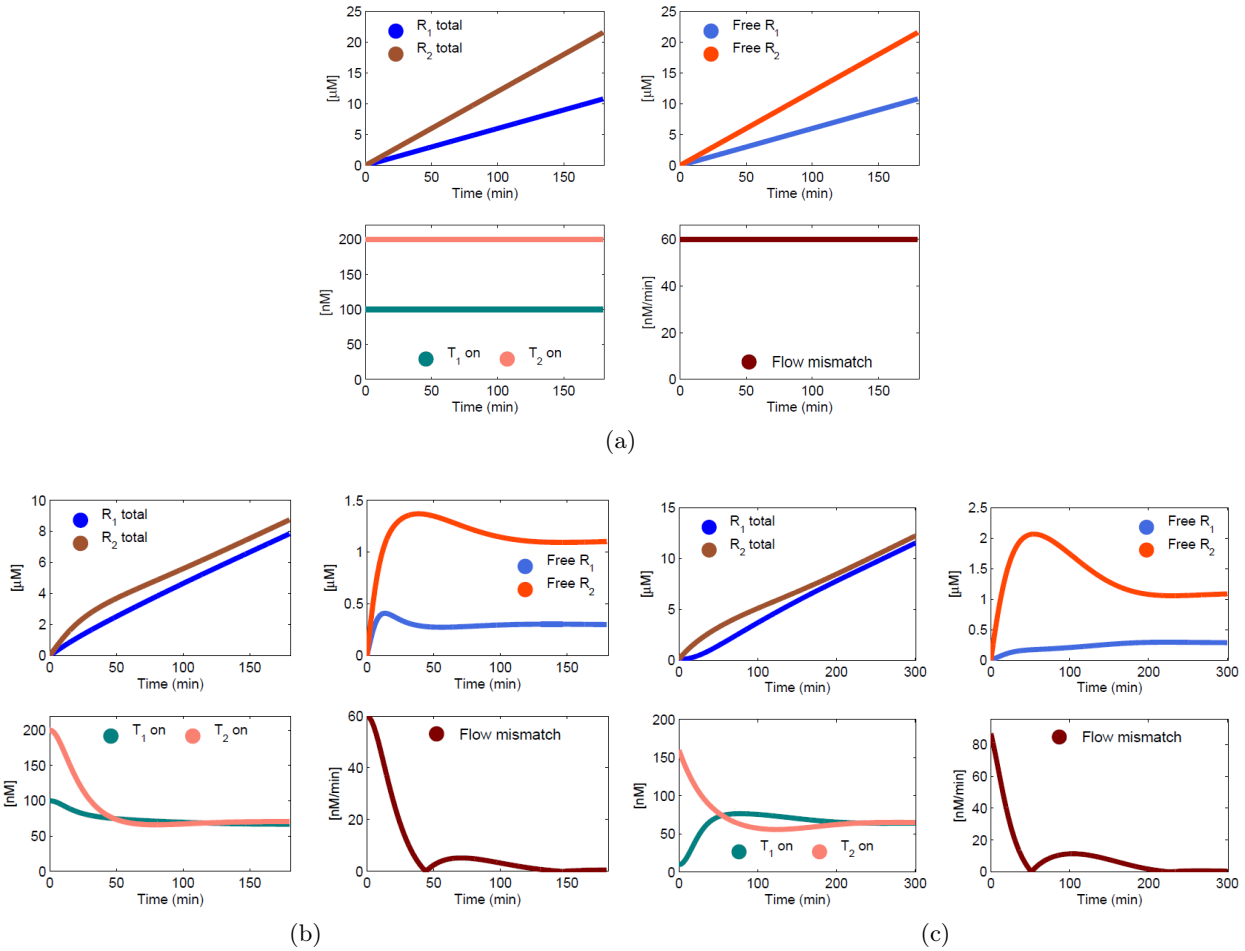

Figure 5: Numerical solutions to the differential equations (a) of the unregulated network, leading to a flux mismatch. (b) of the network regulated by a negative feedback. (c) of the network regulated by a positive feedback. In cases (b) and (c), the flux mismatch observably reduces. Figures reproduced from [3].

implements the best control strategy according to our aim (e.g. maximizing the output flux or minimizing wastes) and what biochemical process generates the most suitable feedback (e.g. mass action kinetics or Hill functions).

Section 2 introduces some basic concept about artificial *in vitro* gene networks (transcriptional circuits). Section 3 is devoted to scaling up flux regulation circuitry to an arbitrary number of genes, according to different product formation schemes; Subsection 3.2 explores negative feedback regulation schemes, Subsection 3.3 instead positive feedback regulation schemes. In Subsection 3.4, the performances of positive and negative feedback schemes are compared and summarized in a table. It is shown that, if we scale up flux regulation circuits, through proper negative or positive feedback loops, flux matching can be achieved with an arbitrary number of genes; moreover, negative feedback seems to have the most interesting and desirable features and so to be worth of further investigations. Section 4 deals with two gene circuits in which positive and negative feedback coexist: through suitable feedback loops, flux matching is achieved as well and the system behavior shows

intermediate features, depending on which of the two feedback constants is the highest. In Section 5, different models to represent feedback are considered. It is shown that mass action kinetics and Hill functions can be both used to model feedback reactions in biochemical systems, yet a different overall behavior is achieved. Section 6 examines more deeply the mass action kinetics negative feedback scheme for rate–regulation circuits, since it appears as the most interesting and easy to implement. In Subsection 6.1 a viable DNA strand implementation is described, based on which in Subsection 6.2 a new model is considered, fitting to the biochemical reactions actually occurring in the system. In Section 7 the project results are summarized and briefly discussed, including implications and future research directions. Finally, Section 8 gives some hints about the routines used for numerical simulations and reports the parameter values used to obtain the graphs shown throughout the paper.

Part of the results are exposed also in [18].

2 Artificial gene networks

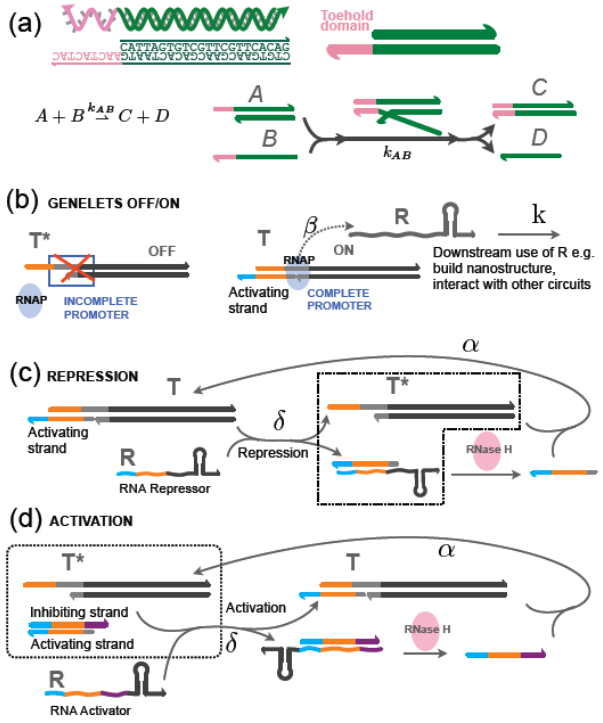

Figure 6: (a) Domain representation of nucleic acids and branch migration (b) On/off state of genelets (c) RNA-mediated repression (d) RNA-mediated activation. Figure reproduced from [18].

Here we introduce artificial *in vitro* gene networks (transcriptional circuits) [13], with the support of Figure 6. Interactions among nucleic acids (DNA and RNA) can be programmed by choosing their sequences (ATCG); strand domains (subsequences of bases) having a particular function, Figure 6 (a), are identified with a specific color (once domain interactions are chosen, automated software tools can be used to find optimal sequences [16]). The arrow on every strand represented in Figure 6 represents the $5'$ end. Reactions in nucleic acid systems occur by hybridization (two single stranded, complementary nucleic acids bind to form a double stranded complex) and by toehold-mediated branch migration [19], exemplified in Figure 6 (a): species A and B interact through the exposed

pink domain and switch to a new, thermodynamically more favorable configuration, creating species D and C. The reaction speed is determined by the length of the toehold domain and is typically tunable in the range 10–10^6/M/s for 1–8 bases toeholds.

Figure 6 (b) introduces artificial genelets; synthetic DNA templates are copied (transcribed) into RNA using T7 RNA polymerase (RNAP); if the RNAP binding region, called promoter, is incomplete (partially single stranded), the genelet is off (T^*). When the double stranded region is reformed by the appropriate DNA activating strand, the genelet is on (T) and RNA output R is produced. The total amount of a genelet is constant, i.e. $[T] + [T^*] = [T^{tot}]$. We assume the enzyme operates in a linear regime, thus R is produced at rate β: $T \xrightarrow{\beta} R + T$. Output R can be used downstream at a rate k, for instance to interact with other RNA species in circuit dynamics or to form nanostructures [2].

In this paper, we describe repression and activation of genelets with a set of aggregate reactions; we obtain intuitive models that bear relevance to general molecular networks.

In Figure 6 (c) we show how a genelet can be repressed by an RNA species R. This pathway is at the basis of the proposed negative feedback circuits. By design, R displaces part of the promoter in the activating strand through toehold-mediated branch migration: $R+T \xrightarrow{\delta} T^*$, where δ is proportional to the length of the toehold domain (cyan domain). We lump the species in the dashed box into species T^*. The inactive gene T^* reverts at rate α to its active form T thanks to the action of RNase H, an enzyme which degrades RNA in RNA/DNA duplexes; R is degraded and the activating strand binds again to the template forming T^*.

In Figure 6 (d) we show how a genelet can be activated by an RNA species R. This pathway is at the basis of the proposed positive feedback designs. In this case, species T^* (dashed box) is comprised of the inactive genelet and a DNA inhibitor-activator complex (the activating strand is sequestered by design). Again, by suitable domain design, R releases the activating–strand through toehold (violet domain) mediated displacement: thus, T^* is converted into T with rate δ (proportional to the toehold length). Now two species coexist: active template T and the complex R·(DNA inhibiting strand). Again, the active gene T reverts to its inactive form T^* at rate α, thanks to the action of RNase H, which releases the inactivating DNA strand.

3 Scaling up rate–regulation circuits

The main goal of the project was to scale up flux regulation circuits to an arbitrary number of genes, generalizing the models proposed in literature for the case of two genes and developing new models for n genes, useful to describe large scale systems with a greater number of interactions.

3.1 Possible schemes

We consider a set of n genelets and different interaction scenarios. We say that genelets are interconnected when their RNA outputs bind to form one or more products. When extending rate–regulator circuitry to an arbitrary number n of genes, the products can be formed in many different ways that lead to different schemes. Fig. 7 shows the schemes considered:

- **single product connection**: all the reagents R_i bind to form a single product, so that the product is always one only, even when n is increasing;
- **"neighbor" connection**: each reagent R_i binds to form a product with only two of the others, namely its neighbors in an imaginary chain, so that the total number of products is n;
- **"handshake" connection**: pairwise, each R_i binds to form a product with every other, so that the total number of products is $n(n-1)/2$.

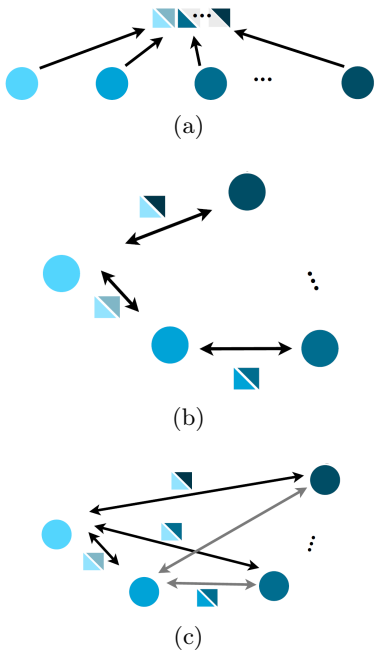

Figure 7: Possible connection schemes with n genes: (a) single product, (b) "neighbor" connection, (c) "handshake" connection.

A *single product* interconnection occurs when a single RNA complex (for instance, a large nanostructure) is formed from the simultaneous interaction of all RNA species.

A network of genelets may be designed to produce different subcomponents, that may later assemble into a larger product. In this scenario, we can take two extreme cases: each RNA participates

in at most two subcomponents (*neighbor* interconnection); each RNA participates in the creation of $n-1$ subcomponents (*handshake* interconnection).

We note that in these three cases, all RNA outputs are used in the same number of complexes. Thus, we would like them to be produced and degraded at comparable rates, given that their downstream utilization is the same. We introduce feedback in these circuits, to compensate imbalances in the concentration of templates and match the transcription rate of the RNA outputs. We will present architectures based on negative and positive feedback, which scale up previously proposed two–gene networks [17, 8].

3.2 Scaling up negative feedback architectures

The negative feedback structure proposed in [3] for the simplest case of two interacting genes can be extended to an arbitrary number of genes, connected one another according to the three different schemes described in 3.1.

3.2.1 Handshake connection

In the handshake connection negative feedback architecture, every gene is interacting pairwise with all the other genes and, if it senses an excess of its product, it down–regulates its own production rate. Here are the chemical reactions and the corresponding differential equations derived through mass action kinetics:

$$
\begin{aligned}
&\mathrm{T_i^* \xrightarrow{\alpha_i} T_i}, \quad [\mathrm{T_i^{tot}}] = [\mathrm{T_i}] + [\mathrm{T_i^*}], && i = 1, ..., n,\\
&\mathrm{T_i \xrightarrow{\beta_i} R_i + T_i}, && \frac{\mathrm{d}[\mathrm{T_i}]}{\mathrm{dt}} = \alpha_\mathrm{i}\left([\mathrm{T_i^{tot}}] - [\mathrm{T_i}]\right) - \delta_\mathrm{i}\,[\mathrm{R_i}][\mathrm{T_i}],\\
&\mathrm{R_i + T_i \xrightarrow{\delta_i} T_i^*}, && \frac{\mathrm{d}[\mathrm{R_i}]}{\mathrm{dt}} = \beta_\mathrm{i}\,[\mathrm{T_i}] - \delta_\mathrm{i}\,[\mathrm{R_i}][\mathrm{T_i}] - \sum_{\mathrm{j=1,\, j\neq i}}^{\mathrm{n}} \mathrm{k_{ij}}\,[\mathrm{R_i}][\mathrm{R_j}],\\
&\mathrm{R_i + R_j \xrightarrow{k_{ij}} P_{ij}}, && \frac{\mathrm{d}[\mathrm{P_{ij}}]}{\mathrm{dt}} = \mathrm{k_{ij}}\,[\mathrm{R_i}][\mathrm{R_j}], \quad \mathrm{i, j = 1, ..., n,\ i \neq j},\\
&[\mathrm{R_i^{tot}}] = [\mathrm{R_i}] + [\mathrm{T_i^*}] + \sum_{\mathrm{j=1,\, j\neq i}}^{\mathrm{n}} [\mathrm{P_{ij}}]. &&
\end{aligned}
$$

The inactive $\mathrm{T_i^*}$ is assumed to naturally revert to its active state with rate α_i, while β_i is the production rate of $\mathrm{R_i}$ and δ_i the strength of the negative feedback. k_{ij} is the generation rate of the product $\mathrm{P_{ij}}$. The set of differential equations was solved numerically in the cases $n = 3$ and 4 and the results are shown in Fig. 9: we can notice that the flow mismatches, shown in the right–bottom panel of figures (a) and (b), considerably reduce with a fast time response. Fig. 10 (a) and (b) show that, if δ increases, concentration and mismatch decrease (the feedback is stronger), while if α increases, they increase ($\mathrm{T_i^*}$ becomes active at a faster rate). This is a common trend for all the negative feedback schemes with n genes.

3.2.2 Neighbor connection

In the neighbor connection negative feedback architecture, the genes can be thought as if they were forming a chain: every gene is interacting with its two neighbors in the chain and, if it senses an excess of its product, it down–regulates its own production rate. Here are the chemical reactions

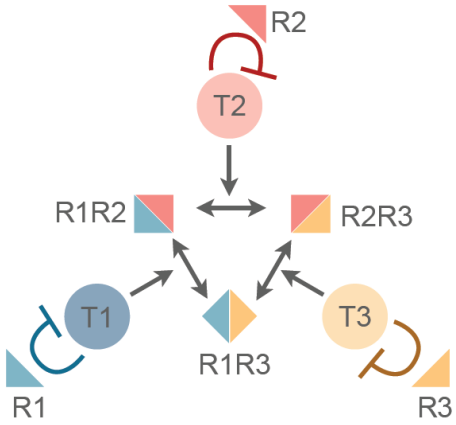

Figure 8: Handshake/neighbor connection negative feedback with 3 genes: graph representation.

and the corresponding differential equations derived through mass action kinetics:

$$
\begin{aligned}
&\mathrm{T_i^* \overset{\alpha_i}{\rightharpoonup} T_i}, \quad [\mathrm{T_i^{tot}}] = [\mathrm{T_i}] + [\mathrm{T_i^*}], && i = 1, ..., n,\\
&\mathrm{T_i \overset{\beta_i}{\rightharpoonup} R_i + T_i}, && \frac{\mathrm{d}[\mathrm{T_i}]}{\mathrm{dt}} = \alpha_\mathrm{i}\left([\mathrm{T_i^{tot}}] - [\mathrm{T_i}]\right) - \delta_\mathrm{i}\,[\mathrm{R_i}][\mathrm{T_i}],\\
&\mathrm{R_i + T_i \overset{\delta_i}{\rightharpoonup} T_i^*}, && \frac{\mathrm{d}[\mathrm{R_i}]}{\mathrm{dt}} = \beta_\mathrm{i}\,[\mathrm{T_i}] - \delta_\mathrm{i}\,[\mathrm{R_i}][\mathrm{T_i}] - \mathrm{k_{i,i-1}}\,[\mathrm{R_i}][\mathrm{R_{i-1}}] - \mathrm{k_{i,i+1}}\,[\mathrm{R_i}][\mathrm{R_{i+1}}],\\
&\mathrm{R_i + R_j \overset{k_{ij}}{\rightharpoonup} P_{ij}}, && \frac{\mathrm{d}[\mathrm{P_{ij}}]}{\mathrm{dt}} = \mathrm{k_{ij}}\,[\mathrm{R_i}][\mathrm{R_j}], \quad \mathrm{i} = 1, ..., \mathrm{n},\ \mathrm{j} = \mathrm{i} - 1, \mathrm{i} + 1,\\
&[\mathrm{R_i^{tot}}] = [\mathrm{R_i}] + [\mathrm{T_i^*}] + [\mathrm{P_{i,i-1}}] + [\mathrm{P_{i,i+1}}].
\end{aligned}
$$

When $i = 1$ we have to consider $i - 1 = n$ and when $i = n$ we have to consider $i + 1 = 1$ to close the chain loop. Note that in the case $n = 3$ this scheme coincides with the handshake connection. The set of differential equations was solved numerically in the case $n = 4$ and the results are shown in Fig. 11. Again, the flow mismatches significantly reduce with a fast time response.

3.2.3 Single product

In the single product negative feedback architecture, all the genes interact to form a unique product and, if each gene senses an excess of its product, it down–regulates its own production rate. Here are the chemical reactions and the corresponding differential equations derived through mass action kinetics:

$$
\begin{aligned}
&\mathrm{T_i^* \overset{\alpha_i}{\rightharpoonup} T_i}, \quad [\mathrm{T_i^{tot}}] = [\mathrm{T_i}] + [\mathrm{T_i^*}], && i = 1, ..., n,\\
&\mathrm{T_i \overset{\beta_i}{\rightharpoonup} R_i + T_i}, && \frac{\mathrm{d}[\mathrm{T_i}]}{\mathrm{dt}} = \alpha_\mathrm{i}\left([\mathrm{T_i^{tot}}] - [\mathrm{T_i}]\right) - \delta_\mathrm{i}\,[\mathrm{R_i}][\mathrm{T_i}],\\
&\mathrm{R_i + T_i \overset{\delta_i}{\rightharpoonup} T_i^*}, && \frac{\mathrm{d}[\mathrm{R_i}]}{\mathrm{dt}} = \beta_\mathrm{i}\,[\mathrm{T_i}] - \delta_\mathrm{i}\,[\mathrm{R_i}][\mathrm{T_i}] - \mathrm{k}\prod_{\mathrm{i}=1}^{\mathrm{n}}[\mathrm{R_i}],\\
&\sum_{\mathrm{i}=1}^{\mathrm{n}} \mathrm{R_i} \overset{\mathrm{k}}{\rightharpoonup} \mathrm{P}, && \frac{\mathrm{d}[\mathrm{P}]}{\mathrm{dt}} = \mathrm{k}\prod_{\mathrm{i}=1}^{\mathrm{n}}[\mathrm{R_i}],\\
&[\mathrm{R_i^{tot}}] = [\mathrm{R_i}] + [\mathrm{T_i^*}] + [\mathrm{P}].
\end{aligned}
$$

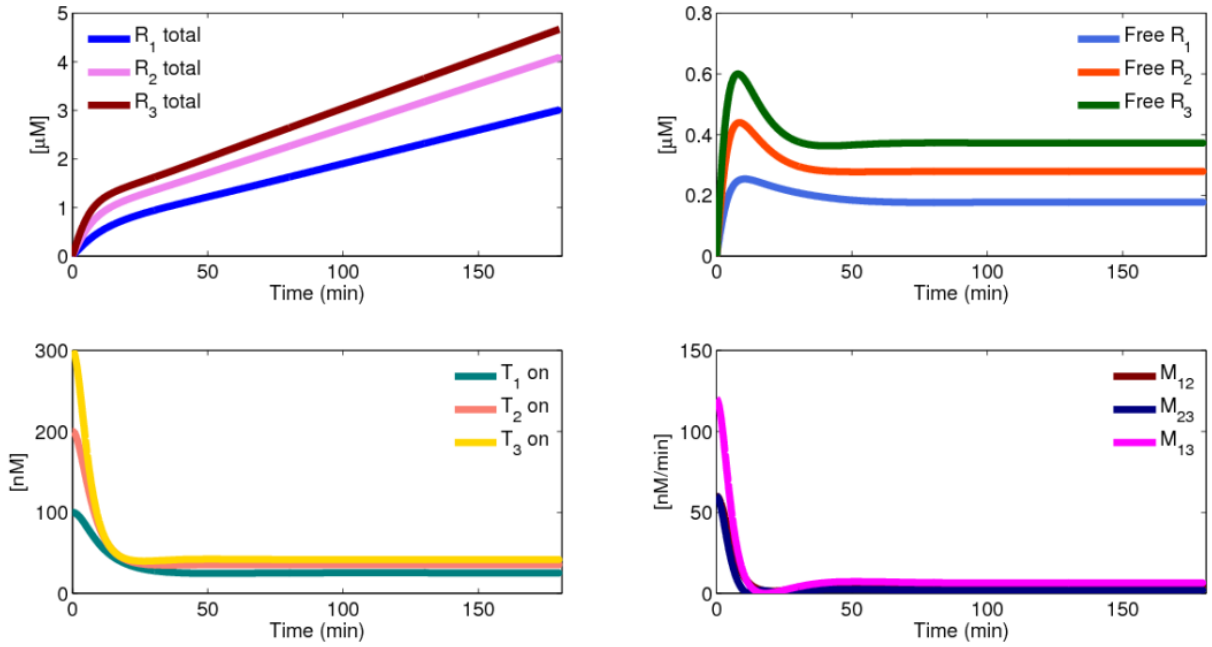

(a)

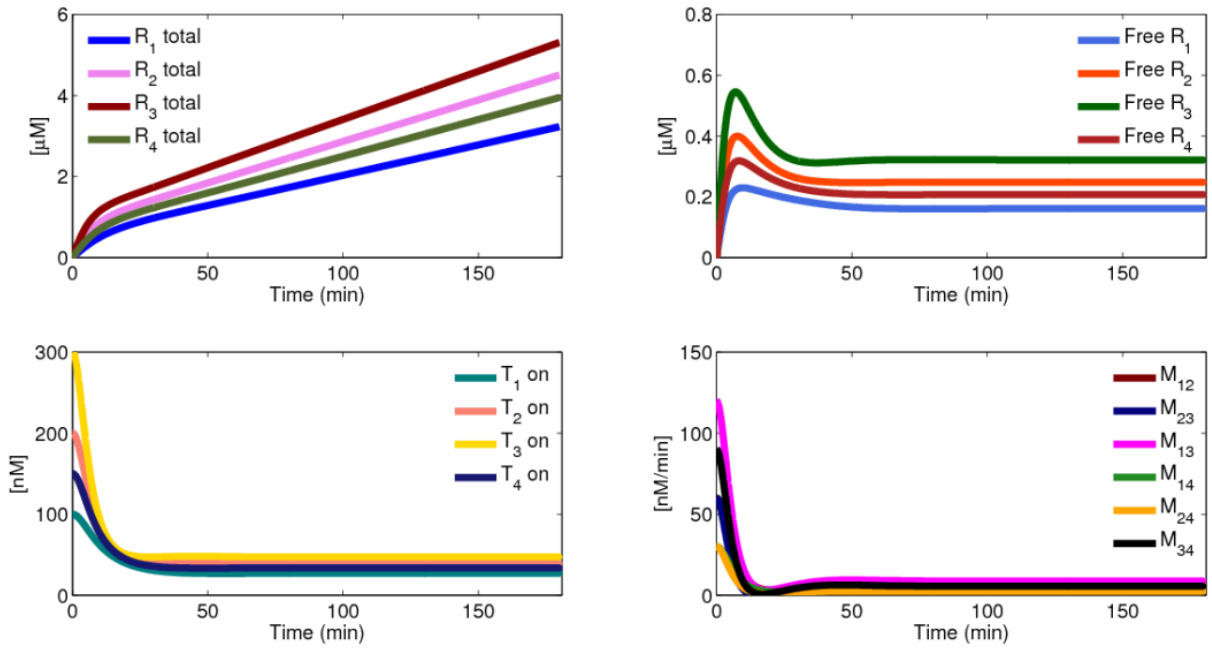

(b)

Figure 9: Handshake/neighbor connection negative feedback with 3 genes: (a) numerical ODE solutions. Handshake connection negative feedback with 4 genes: (b) numerical ODE solutions.

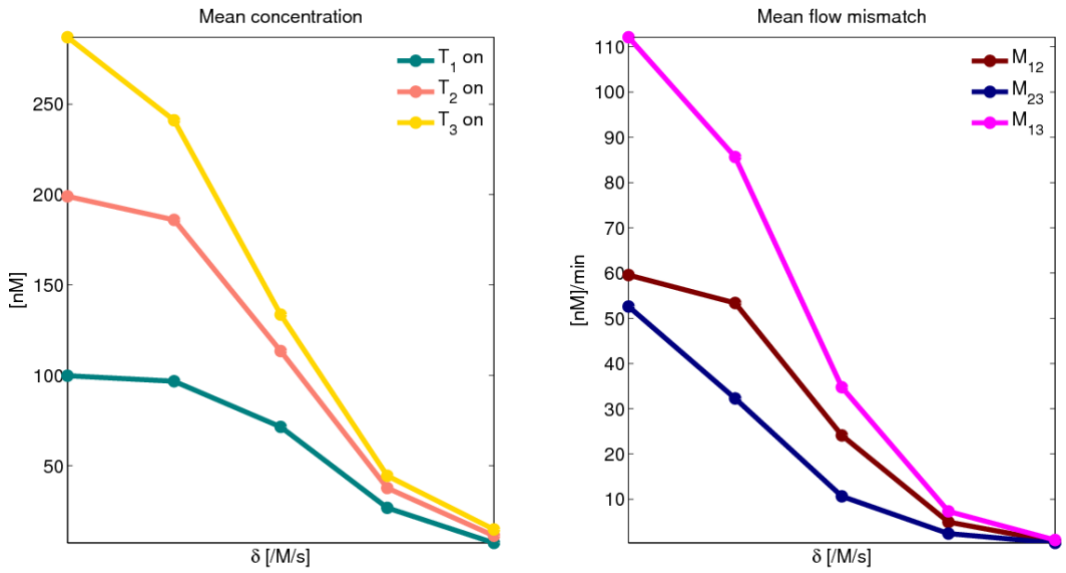

(a)

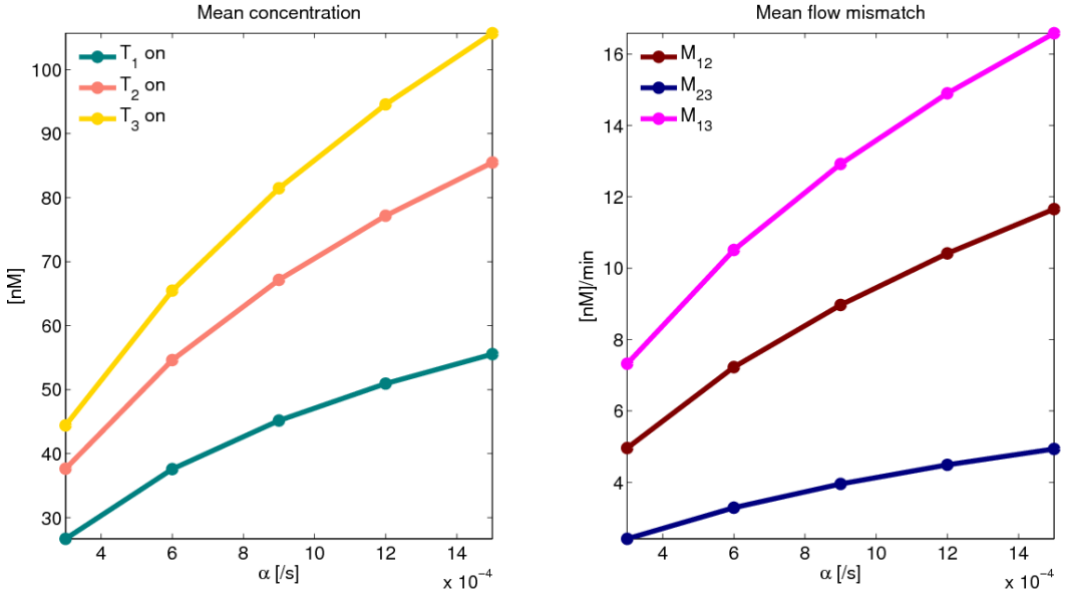

(b)

Figure 10: Handshake connection negative feedback with 3 genes: steady state values of mean concentrations and mean flow mismatches shown as a function of (a) δ and (b) α.

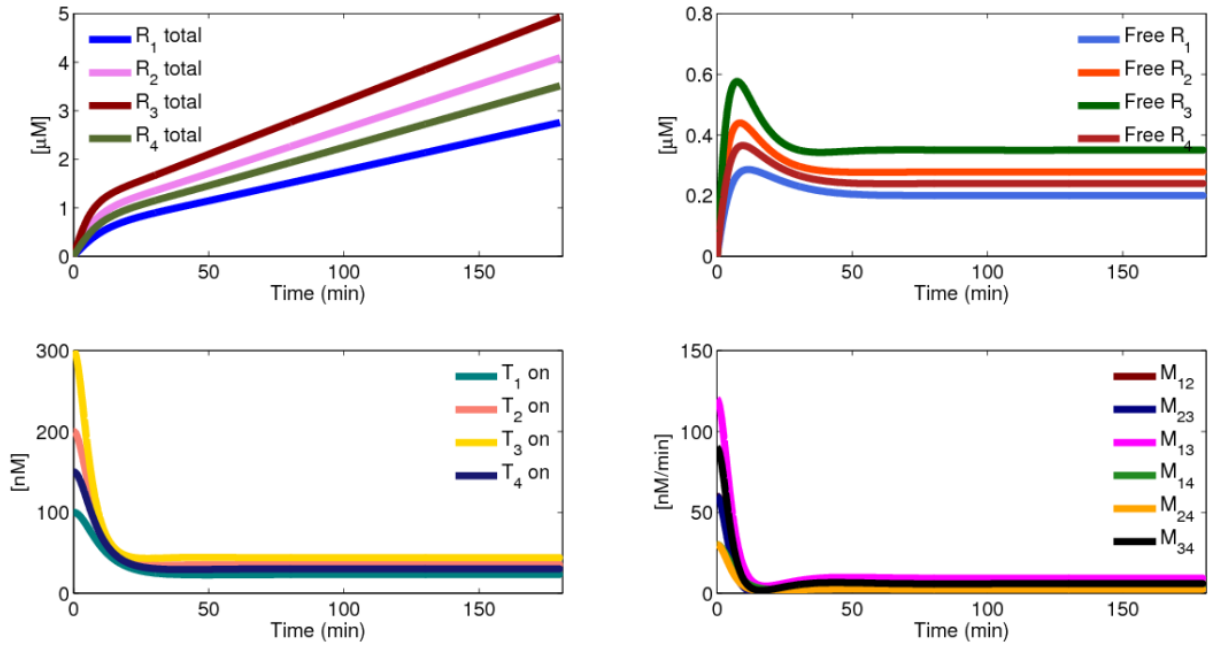

(a)

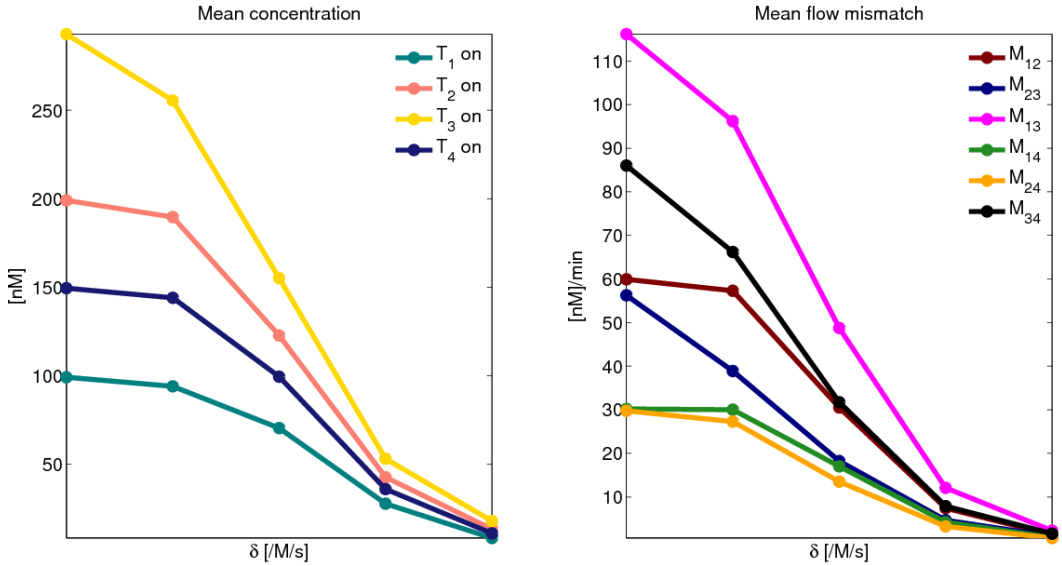

(b)

Figure 11: Neighbor connection negative feedback with 4 genes: (a) numerical ODE solutions, (b) steady state values of mean concentrations and mean flow mismatches shown as a function of δ.

k is the generation rate of the unique product P. The results of numerical simulation with three and four genes are shown in Fig. 12 and 13. The mismatches reduce as well, but the time response is slightly slower than in the two cases previously shown, even though it is quite fast anyway.

3.2.4 Negative feedback architectures: a survey

Negative feedback architectures for rate–regulation have many remarkable features: they have a very fast time response, they are modular and easy to scale up to a simple general structure, because every gene is controlling its own production rate. Yet it is worth noting that negative feedback loops optimize flux matching for avoiding wastes, but do not maximize the output production rate, that can reach low levels. That's why this type of scheme is most suitable to adjust the production rate of a species to a level close to the flux effectively needed, avoiding accumulation of potentially harmful excess, in the case of genes in low demand. Because of their interesting properties and effectiveness, negative feedback rate–regulators have been analyzed more in deep and a possible experimental implementation of these architectures has been studied (see Section 6).

3.3 Scaling up positive feedback architectures

The positive feedback structure proposed in [3] for the simplest case of two interacting genes has been extended to an arbitrary number of genes, connected one another according to the three different schemes described in 3.1.

3.3.1 Handshake connection

In the handshake connection positive feedback architecture, every gene is interacting pairwise with all the other genes and, if one reagent is in excess, it will increase the production rate of all the other reagents it is reacting with. Here are the chemical reactions and the corresponding differential equations derived through mass action kinetics:

$$
\begin{aligned}
&\mathrm{T_i} \xrightarrow{\alpha_i} \mathrm{T_i^*}, \quad [\mathrm{T_i^{tot}}] = [\mathrm{T_i}] + [\mathrm{T_i^*}], && i = 1, ..., n,\\
&\mathrm{T_i} \xrightarrow{\beta_i} \mathrm{R_i} + \mathrm{T_i}, && \frac{\mathrm{d}[\mathrm{T_i}]}{\mathrm{dt}} = -\alpha_\mathrm{i}\,[\mathrm{T_i}] + \sum_{\mathrm{j}\neq\mathrm{i}} \delta_\mathrm{ij}\,[\mathrm{R_j}]([\mathrm{T_i^{tot}}] - [\mathrm{T_i}]),\\
&\mathrm{R_i} + \mathrm{T_j^*} \xrightarrow{\delta_{ij}} \mathrm{T_j}, && \frac{\mathrm{d}[\mathrm{R_i}]}{\mathrm{dt}} = \beta_\mathrm{i}\,[\mathrm{T_i}] - \sum_{\mathrm{j}\neq\mathrm{i}} \mathrm{k_{ij}}\,[\mathrm{R_i}][\mathrm{R_j}] - \sum_{\mathrm{j}\neq\mathrm{i}} \delta_\mathrm{ji}\,[\mathrm{R_i}]([\mathrm{T_j^{tot}}] - [\mathrm{T_j}]),\\
&\mathrm{R_i} + \mathrm{R_j} \xrightarrow{\mathrm{k_{ij}}} \mathrm{P_{ij}}, && \frac{\mathrm{d}[\mathrm{P_{ij}}]}{\mathrm{dt}} = \mathrm{k_{ij}}\,[\mathrm{R_i}][\mathrm{R_j}], \quad \mathrm{i,j} = 1, ..., \mathrm{n},\ \mathrm{i} \neq \mathrm{j},\\
&[\mathrm{R_i^{tot}}] = [\mathrm{R_i}] + \sum_{\mathrm{j}=1,\,\mathrm{j}\neq\mathrm{i}}^{\mathrm{n}} [\mathrm{T_j}] + \sum_{\mathrm{j}=1,\,\mathrm{j}\neq\mathrm{i}}^{\mathrm{n}} [\mathrm{P_{ij}}].
\end{aligned}
$$

The active $\mathrm{T_i}$ is assumed to naturally inactivate with rate α_i, while β_i is the production rate of $\mathrm{R_i}$ and δ_{ij} the strength of the positive feedback on gene i due to gene j. k_{ij} is the generation rate of the product $\mathrm{P_{ij}}$. The set of differential equations was solved numerically in the case $n = 3$ and the results are shown in Fig. 15: we can notice that the flow mismatches, shown in the right–bottom panel of figure (a), considerably reduce, but the response time is longer than in the negative feedback case. Fig. 15 (b) and (c) show that, if δ increases, concentration and mismatch increase (the feedback is stronger and the system becomes instable); while if α increases, they decrease ($\mathrm{T_i}$ becomes inactive at a faster rate), which is a common trend for all the positive feedback schemes with n genes.

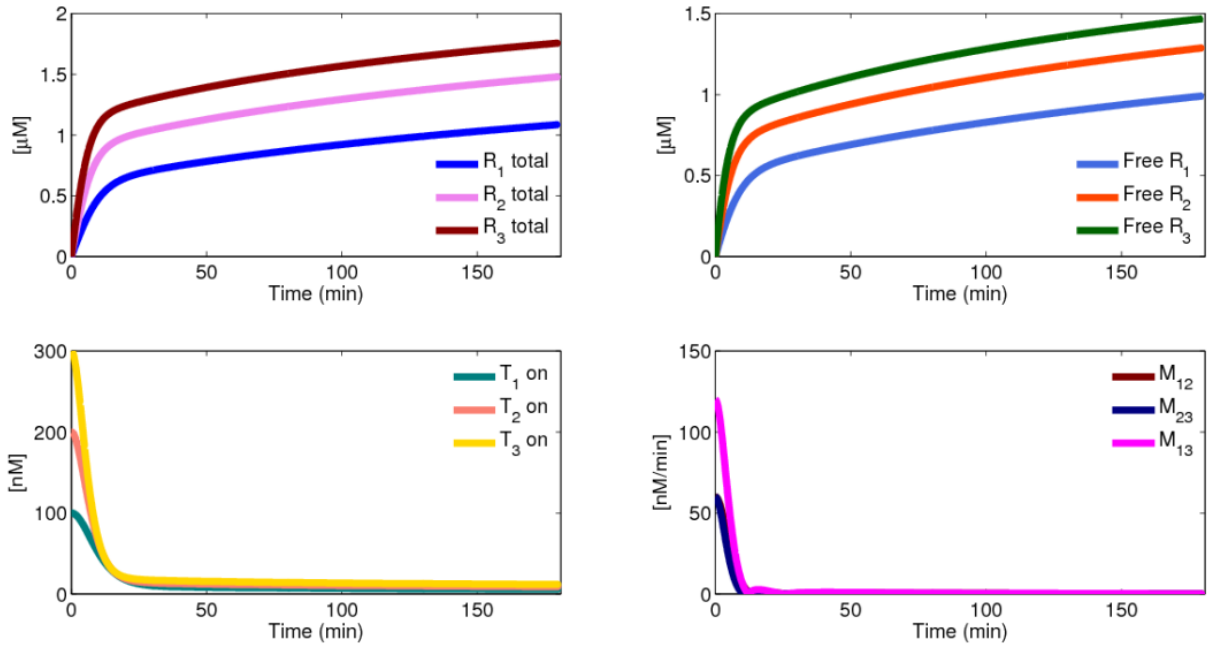

(a)

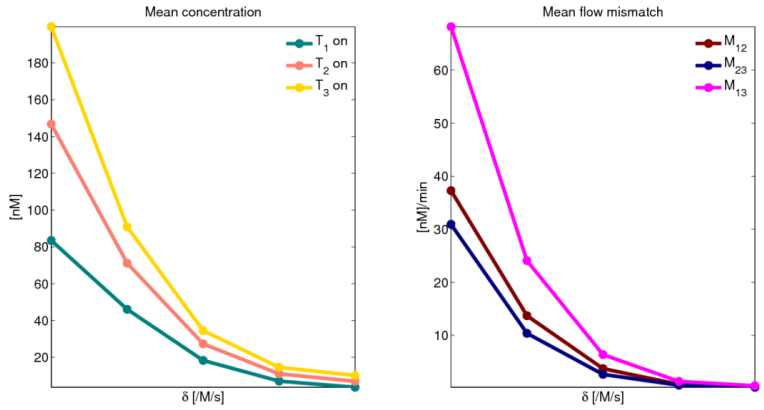

(b)

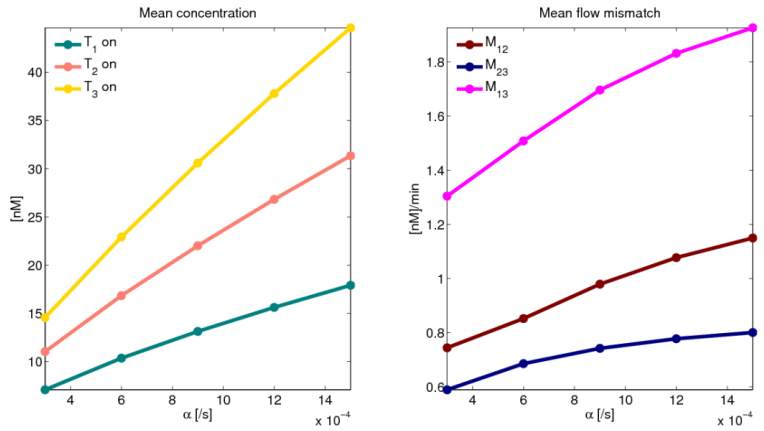

(c)

Figure 12: Single product negative feedback with 3 genes: (a) numerical ODE solutions; steady state values of mean concentrations and mean flow mismatches shown as a function of (b) δ, (c) α.

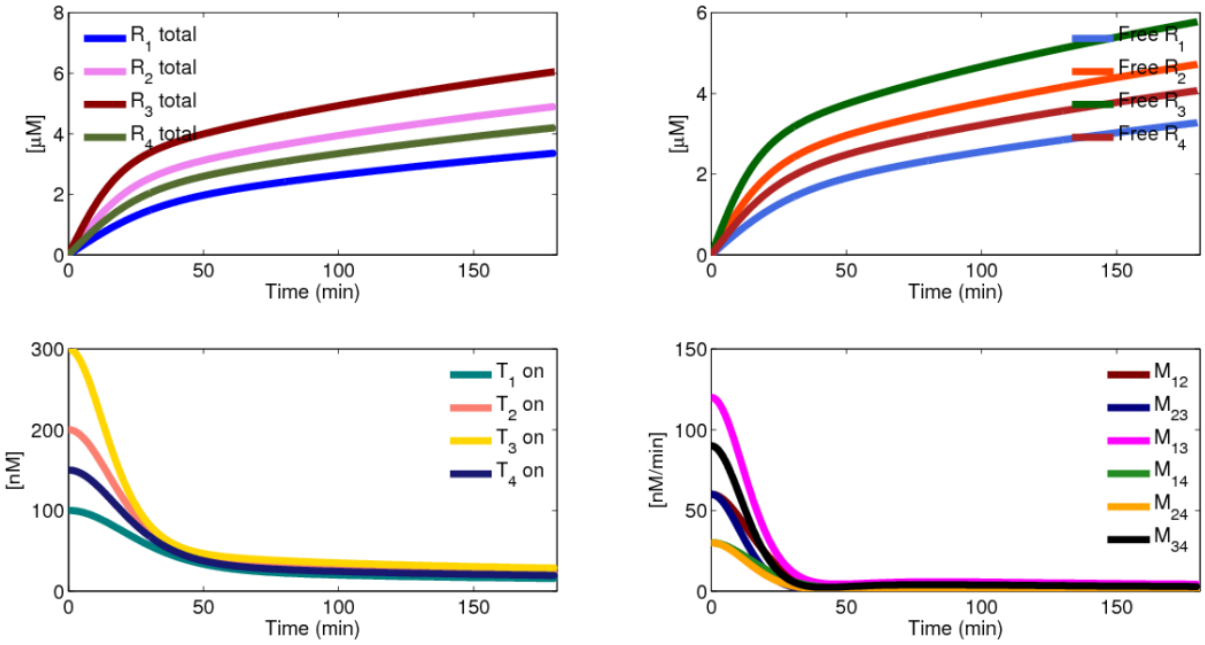

(a)

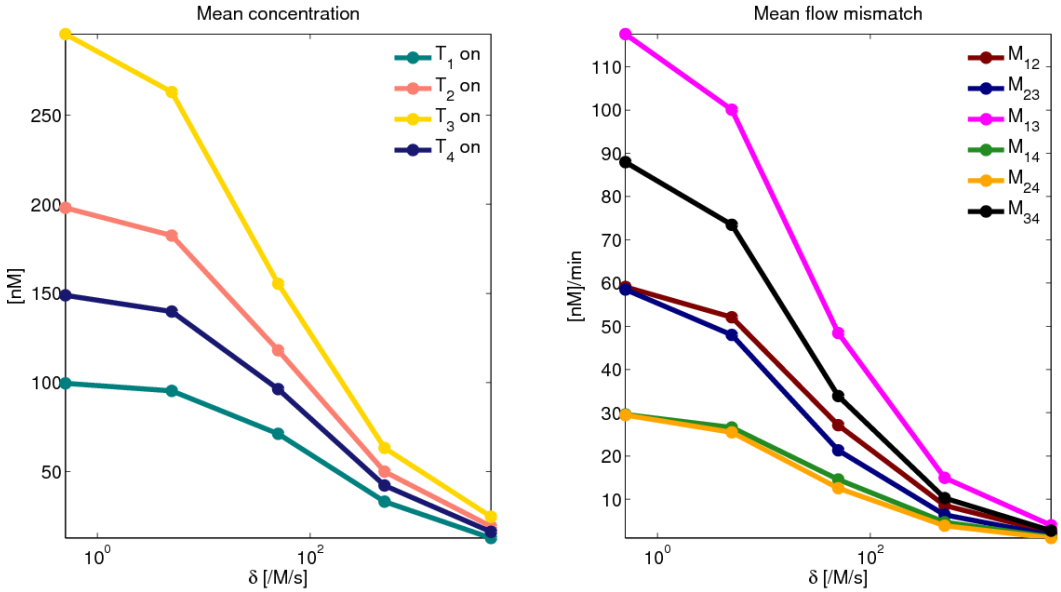

(b)

Figure 13: Single product negative feedback with 4 genes: (a) numerical ODE solutions, (b) steady state values of mean concentrations and mean flow mismatches shown as a function of δ.

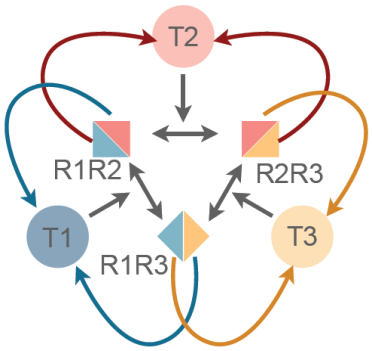

Figure 14: Handshake/neighbor connection positive feedback with 3 genes: graph representation.

3.3.2 Neighbor connection

In the neighbor connection positive feedback architecture, the genes can be thought as if they were forming a chain: every gene is interacting with its two neighbors in the chain and, if one reagent is in excess, it will increase the production rate of the two neighboring reagents it is reacting with. Here are the chemical reactions and the corresponding differential equations derived through mass action kinetics:

$$\mathrm{T_i} \overset{\alpha_i}{\rightharpoonup} \mathrm{T_i^*}, \quad [\mathrm{T_i^{tot}}] = [\mathrm{T_i}] + [\mathrm{T_i^*}], \qquad i = 1, ..., n,$$

$$\mathrm{T_i} \overset{\beta_i}{\rightharpoonup} \mathrm{R_i} + \mathrm{T_i}, \qquad \frac{\mathrm{d}[\mathrm{T_i}]}{\mathrm{dt}} = -\alpha_\mathrm{i}\,[\mathrm{T_i}] + \sum_{\mathrm{j=i\pm1}} \delta_\mathrm{ij}\,[\mathrm{R_j}]([\mathrm{T_i^{tot}}] - [\mathrm{T_i}]),$$

$$\mathrm{R_i} + \mathrm{T_j^*} \overset{\delta_{ij}}{\rightharpoonup} \mathrm{T_j}, \qquad \frac{\mathrm{d}[\mathrm{R_i}]}{\mathrm{dt}} = \beta_\mathrm{i}\,[\mathrm{T_i}] - \sum_{\mathrm{j=i\pm1}} \mathrm{k_{i,j}}\,[\mathrm{R_i}][\mathrm{R_j}] - \sum_{\mathrm{j=i\pm1}} \delta_\mathrm{ji}\,[\mathrm{R_i}]([\mathrm{T_j^{tot}}] - [\mathrm{T_j}]),$$

$$\mathrm{R_i} + \mathrm{R_j} \overset{\mathrm{k_{ij}}}{\rightharpoonup} \mathrm{P_{ij}}, \qquad \frac{\mathrm{d}[\mathrm{P_{ij}}]}{\mathrm{dt}} = \mathrm{k_{ij}}\,[\mathrm{R_i}][\mathrm{R_j}], \quad \mathrm{i} = 1, ..., \mathrm{n},\ \mathrm{j} = \mathrm{i} - 1, \mathrm{i} + 1,$$

$$[\mathrm{R_i^{tot}}] = [\mathrm{R_i}] + \sum_{\mathrm{j=i\pm1}} [\mathrm{T_j}] + [\mathrm{P_{i,i-1}}] + [\mathrm{P_{i,i+1}}].$$

When $i = 1$ we have to consider $i - 1 = n$ and when $i = n$ we have to consider $i + 1 = 1$ to close the chain loop. Note that in the case $n = 3$ this scheme coincides with the handshake connection.

3.3.3 Single product

In the single product positive feedback architecture, all the genes interact to form a unique product and, if one reagent is in shortage, its production rate will be enhanced by the others. Here are the chemical reactions and the corresponding differential equations derived through mass action

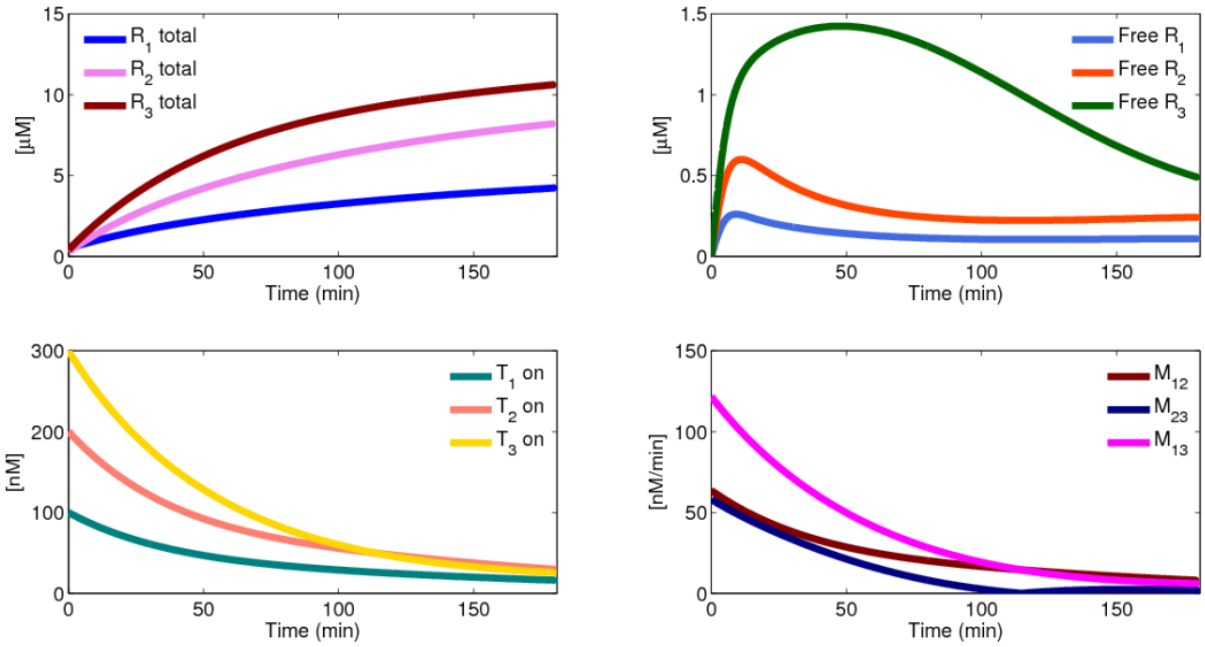

(a)

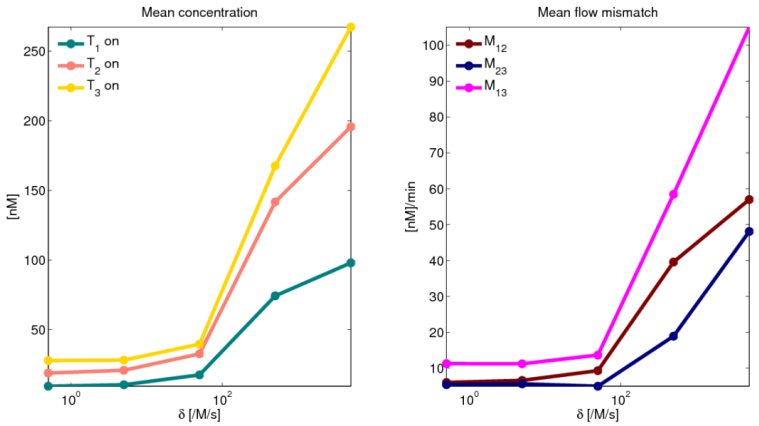

(b)

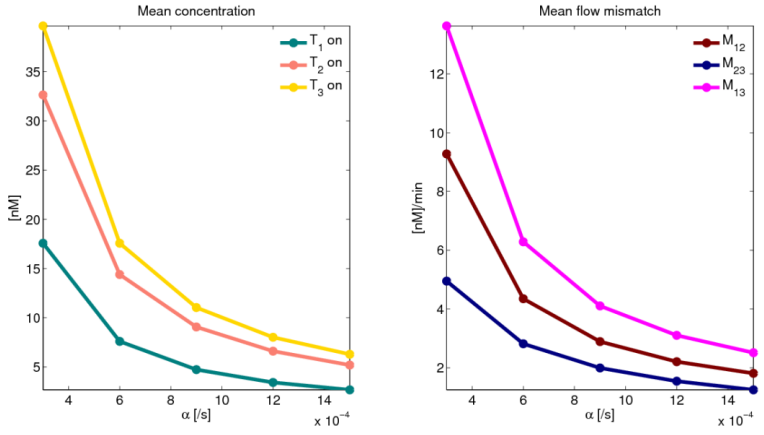

(c)

Figure 15: Handshake/neighbor connection positive feedback with 3 genes: (a) numerical ODE solutions. Steady state values of mean concentrations and mean flow mismatches shown as a function of (b) δ, (c) α.

kinetics:

$$
\begin{aligned}
&\mathrm{T_i} \overset{\alpha_i}{\rightharpoonup} \mathrm{T_i^*}, \quad [\mathrm{T_i^{tot}}] = [\mathrm{T_i}] + [\mathrm{T_i^*}], && i = 1, ..., n, \\
&\mathrm{T_i} \overset{\beta_i}{\rightharpoonup} \mathrm{R_i} + \mathrm{T_i}, && \frac{\mathrm{d}[\mathrm{T_i}]}{\mathrm{dt}} = -\alpha_\mathrm{i}\,[\mathrm{T_i}] + \delta_\mathrm{i}\,([\mathrm{T_i^{tot}}] - [\mathrm{T_i}]) \prod_{\mathrm{j}\neq\mathrm{i}} [\mathrm{R_j}], \\
&\sum_{\mathrm{i}=1}^{\mathrm{n}} \mathrm{R_i} \overset{\mathrm{k}}{\rightharpoonup} \mathrm{P}, && \frac{\mathrm{d}[\mathrm{R_i}]}{\mathrm{dt}} = \beta_\mathrm{i}\,[\mathrm{T_i}] - \mathrm{k} \prod_{\mathrm{i}=1}^{\mathrm{n}} [\mathrm{R_i}] - \delta_\mathrm{i}\,[\mathrm{R_i}] \prod_{\mathrm{j}\neq\mathrm{i}} ([\mathrm{T_j^{tot}}] - [\mathrm{T_j}]), \\
&[\mathrm{R_i^{tot}}] = [\mathrm{R_i}] + \sum_{\mathrm{j}=1,\,\mathrm{j}\neq\mathrm{i}}^{\mathrm{n}} [\mathrm{T_j}] + [\mathrm{P}], && \frac{\mathrm{d}[\mathrm{P}]}{\mathrm{dt}} = \mathrm{k} \prod_{\mathrm{i}=1}^{\mathrm{n}} [\mathrm{R_i}].
\end{aligned}
$$

k is the generation rate of the unique product P and δ_i is the strength of the positive feedback on gene i due to all the others. The results of numerical simulation with three genes are shown in Fig. 16 and it is interesting to observe that, in this particular case, mean concentrations and flow mismatches are independent of δ.

3.3.4 Positive feedback architectures: a survey

Positive feedback architectures for rate–regulation maximize the overall output rate of production. Yet they have a much slower time response, with respect to negative feedback architectures, and above all the feedback constant must be very small not to cause instability. They are not so easy to scale up: the number of interactions is growing with n, because each gene is controlled by all the others with which it works to form products. Therefore, this type of scheme is most suitable to adjust the production rate when a high amount of product is required, in the case of genes in high demand, but in general it is necessary to be careful to avoid problems of instability.

3.4 Negative and positive feedback: a comparison

If we compare the two feedback schemes, we notice that the negative feedback has a lot of interesting features: it has a fast time response, it is easy to scale up because each gene controls its own production rate, it is stabilizing for the system. Yet it is not meant to maximize the output production rate and thus the overall output flux may reach low levels. The positive feedback, instead, has a slower response time, is more difficult to scale up because each gene is controlled by the others and so increasing the number of genes involved leads to a growing number of interactions, the feedback constant must be kept very small not to lead the system to instability. Yet the overall output flux is maximized. So negative feedback is the best control strategy, if genes are not highly required, and it avoids the accumulation of potentially harmful excess of unused reagents; while positive feedback is the best strategy for genes in high demand, since it maximizes the production rate.

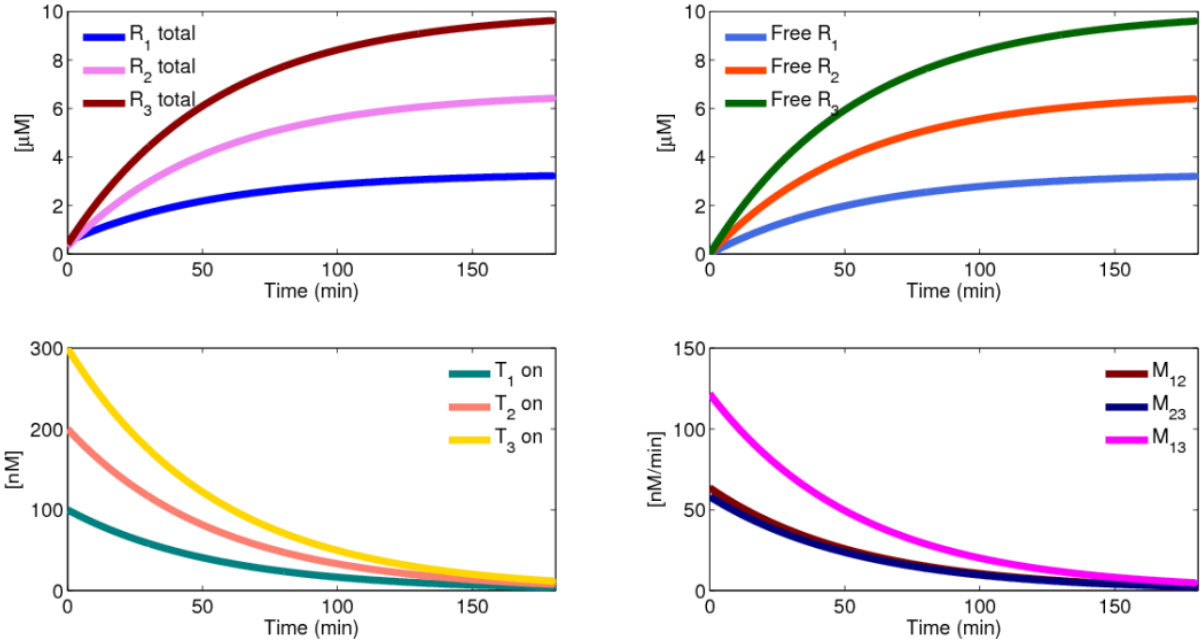

(a)

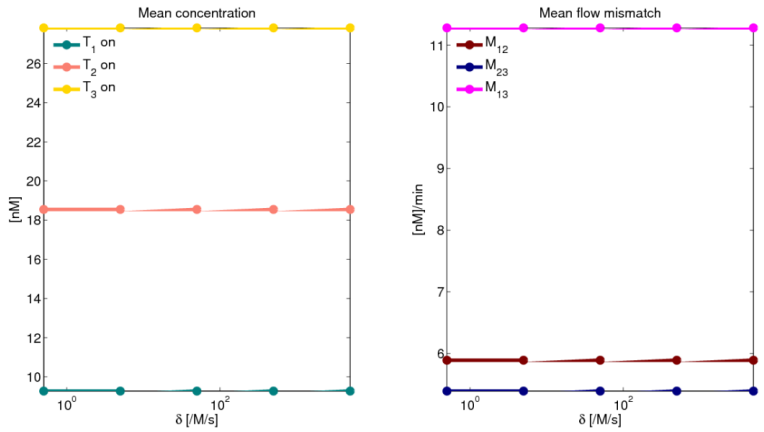

(b)

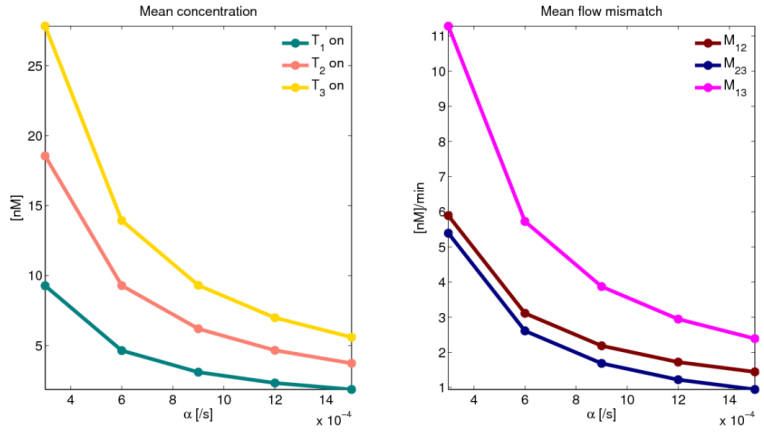

(c)

Figure 16: Single product positive feedback with 3 genes: (a) numerical ODE solutions; steady state values of mean concentrations and mean flow mismatches shown as a function of (b) δ, (c) α.

	Negative feedback	*Positive feedback*
When δ increases	mismatch decreases	mismatch increases
When α increases	mismatch increases	mismatch decreases
Stability	stable system	feedback constants not small enough can lead to instability
Time response	fast	slower
Scaling up	easy (each gene controls its own production rate)	more difficult (each gene controlled by the others: growing number of interactions)
Production rate	may reach low levels	maximized
Best control strategy for	genes not highly required	genes in high demand

4 Both positive and negative feedback with two genes

It may be interesting to see what happens if in the system considered both positive and negative feedback loops are present. To examine this aspect, we study the simple two gene system and we assume that only one of the two spontaneous conversion rates $\alpha_{i,pos}$ (inactivation of T_i) and $\alpha_{i,neg}$ (activation of T_i^*) is different from zero. The resulting ODE system is

$$\frac{d[T_i]}{dt} = -\alpha_{i,pos}\,[T_i] + (\alpha_{i,neg} + \delta_{ij}\,[R_j])\,([T_i^{tot}] - [T_i]) - \delta_i\,[R_i]\,[T_i]$$
$$\frac{d[R_i]}{dt} = \beta_i\,[T_i] - k\,[R_1][R_2] - \delta_i\,[R_i]\,[T_i] - \delta_{ji}\,[R_i]([T_j^{tot}] - [T_j])$$
$$\frac{d[P]}{dt} = k\,[R_1][R_2]$$
where $i, j = 1, 2$; $\alpha_{i,pos}$ or $\alpha_{i,neg}$ must be zero

By means of numerical simulation, it is possible to notice that the system shows an intermediate behavior, which is more similar to pure negative or positive feedback, according to which feedback constant δ is the strongest. Figures 18, 19, 20 and 21 show some plots obtained with different values of the feedback constant δ for positive and negative feedback, in both cases $\alpha_{i,pos} = 0$ and $\alpha_{i,neg} = 0$.

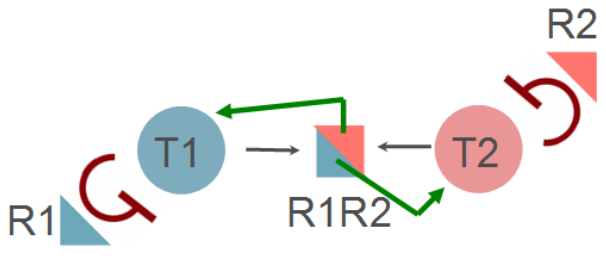

Figure 17: System with both positive and negative feedback: graph representation.

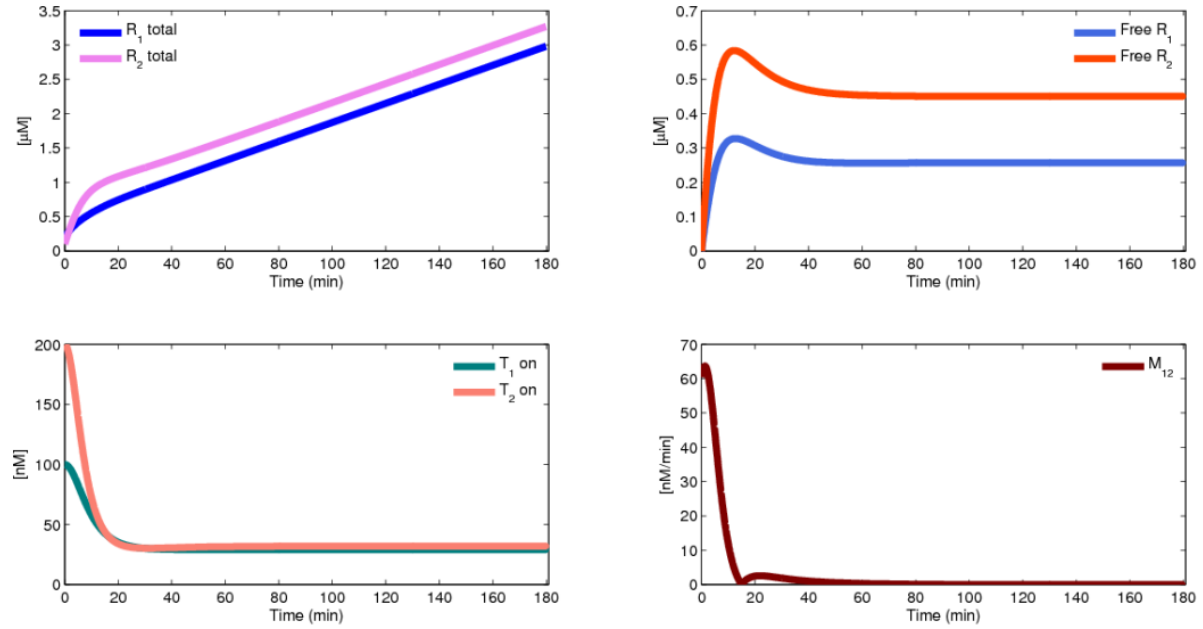

(a)

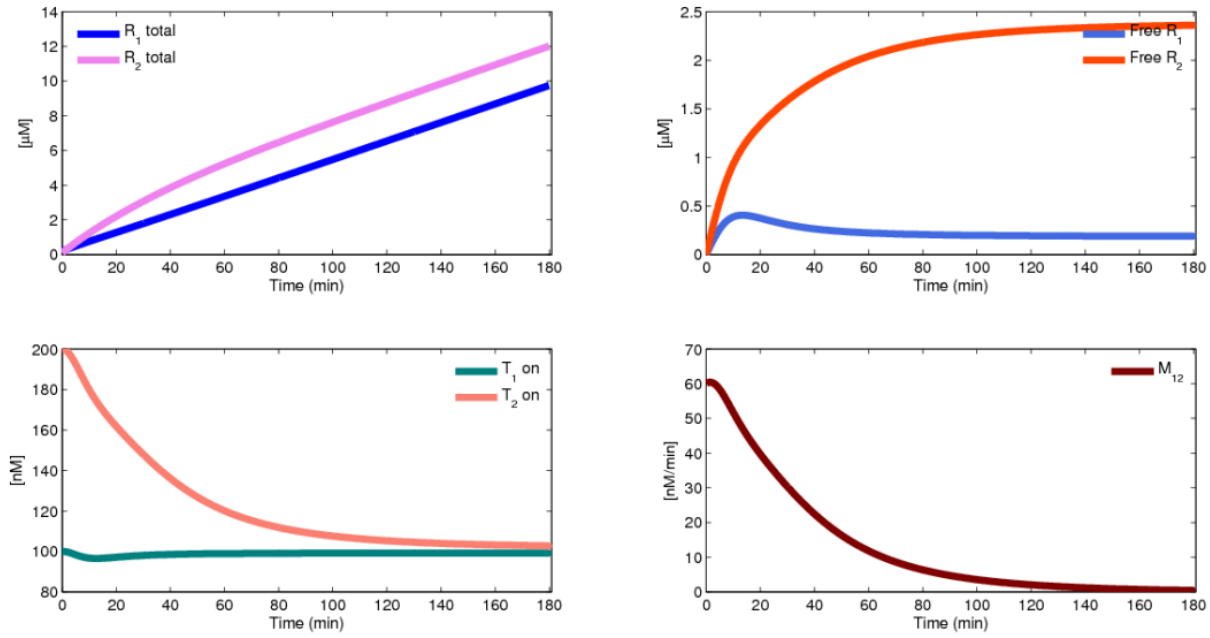

(b)

Figure 18: System with both positive and negative feedback. If $\alpha_{\text{i,neg}} \neq 0$: numerical ODE solutions when (a) δ negative is greater than δ positive, (b) δ positive is greater than δ negative.

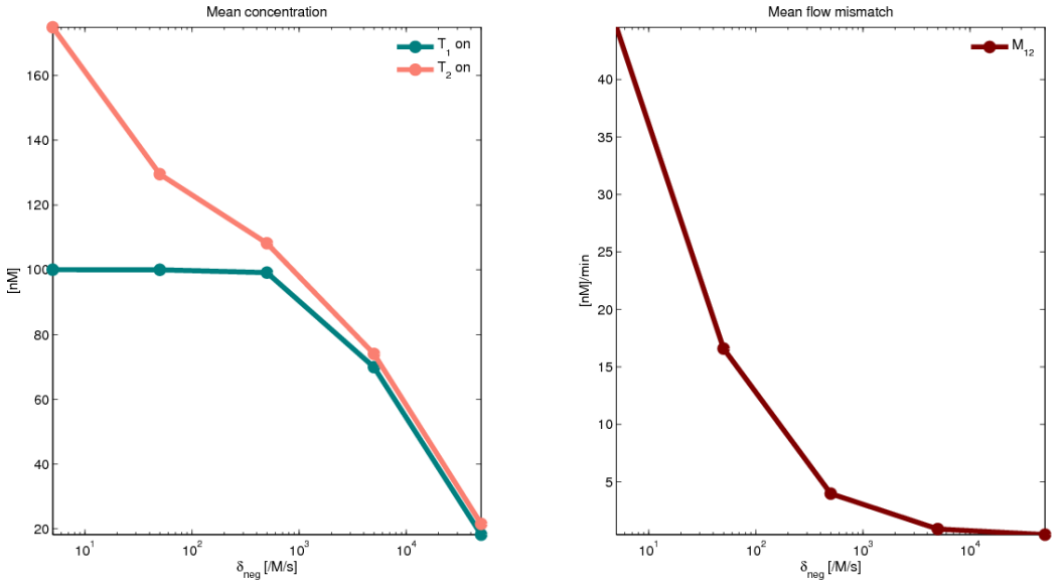

(a)

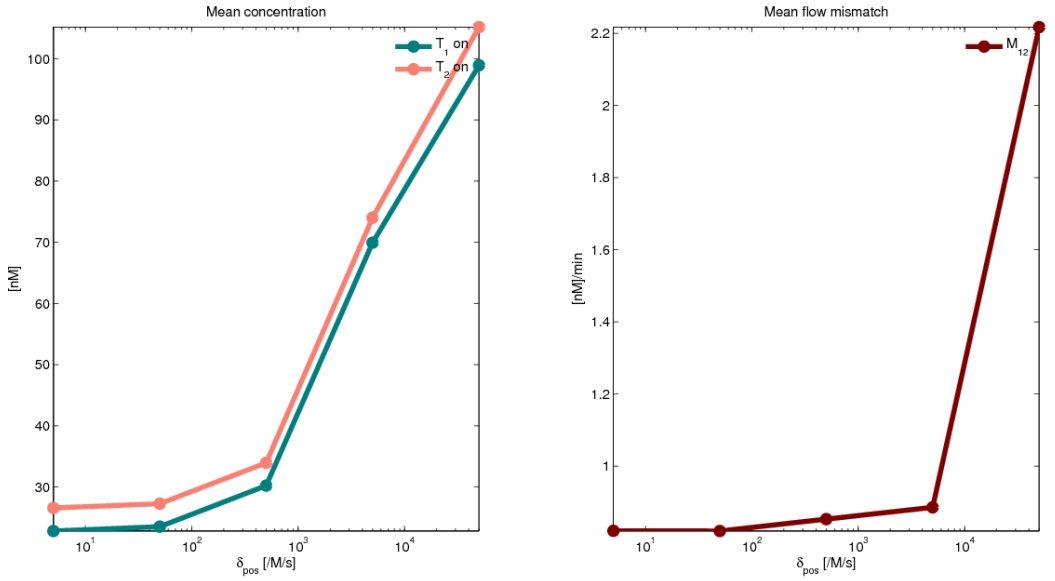

(b)

Figure 19: System with both positive and negative feedback. If $\alpha_{\mathrm{i,neg}} \neq 0$: steady state values of mean concentrations and mean flow mismatches decrease (a) if δ negative increases or (b) if δ positive decreases.

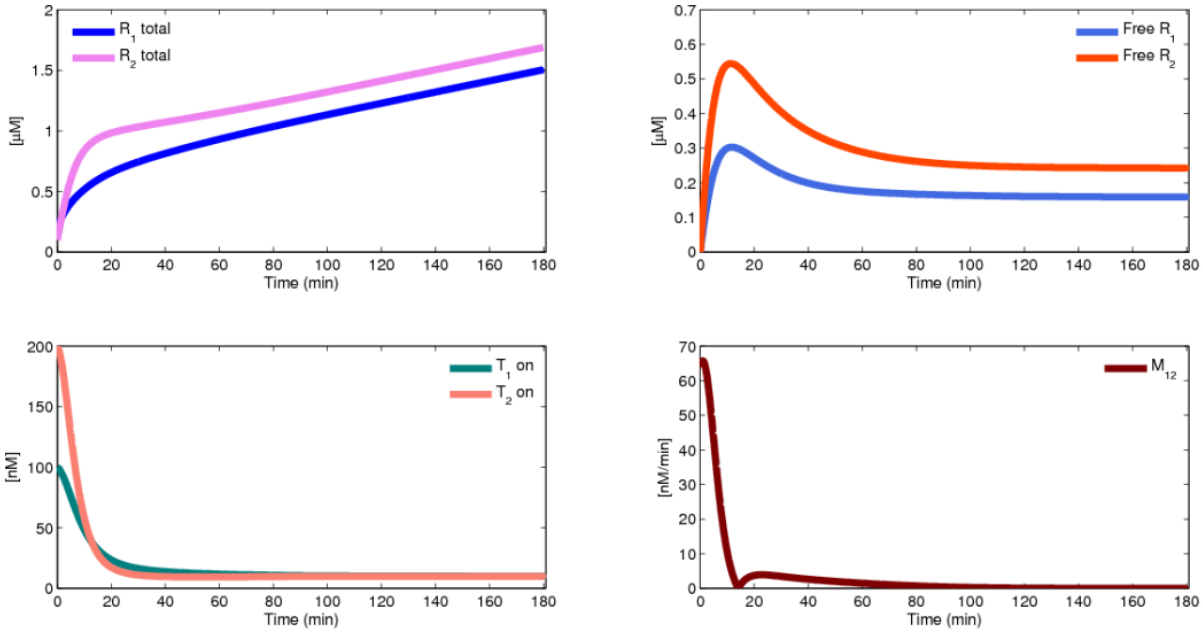

(a)

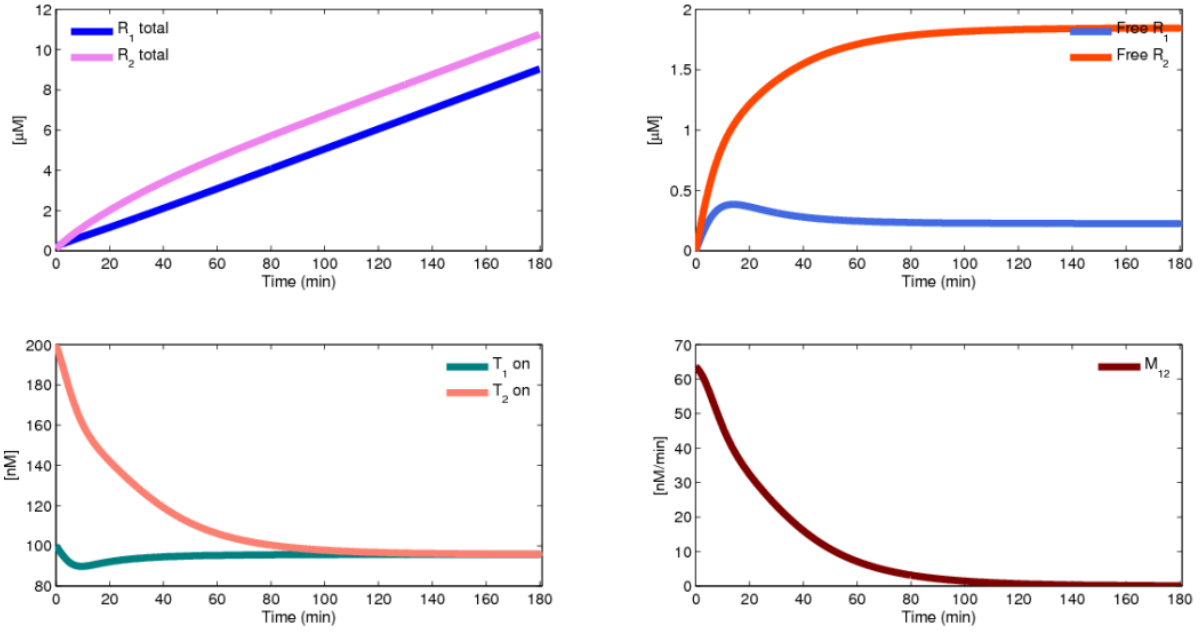

(b)

Figure 20: System with both positive and negative feedback. If $\alpha_{\mathrm{i,pos}} \neq 0$: numerical ODE solutions when (a) δ negative is greater than δ positive, (b) δ positive is greater than δ negative.

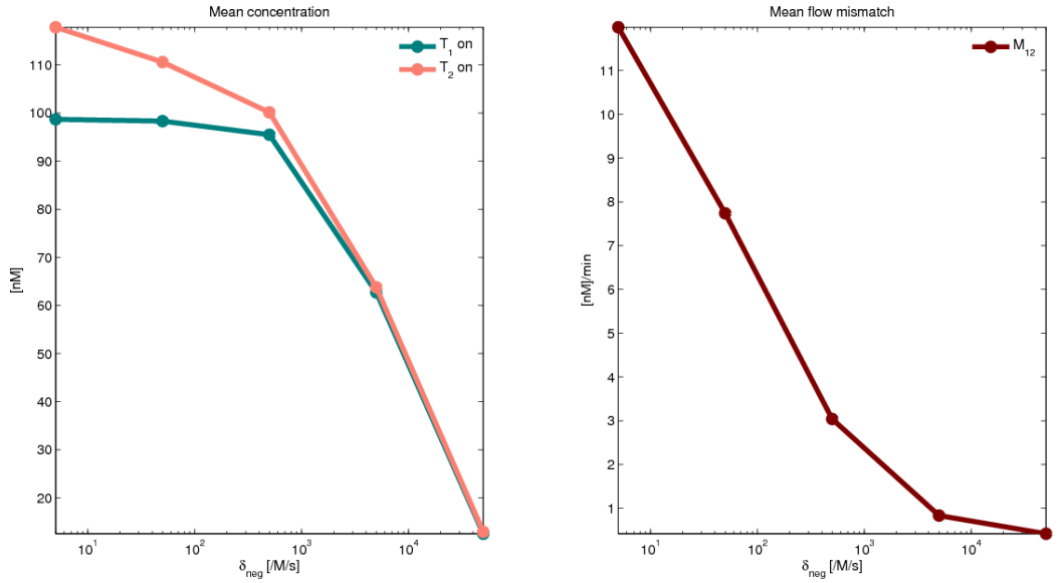

(a)

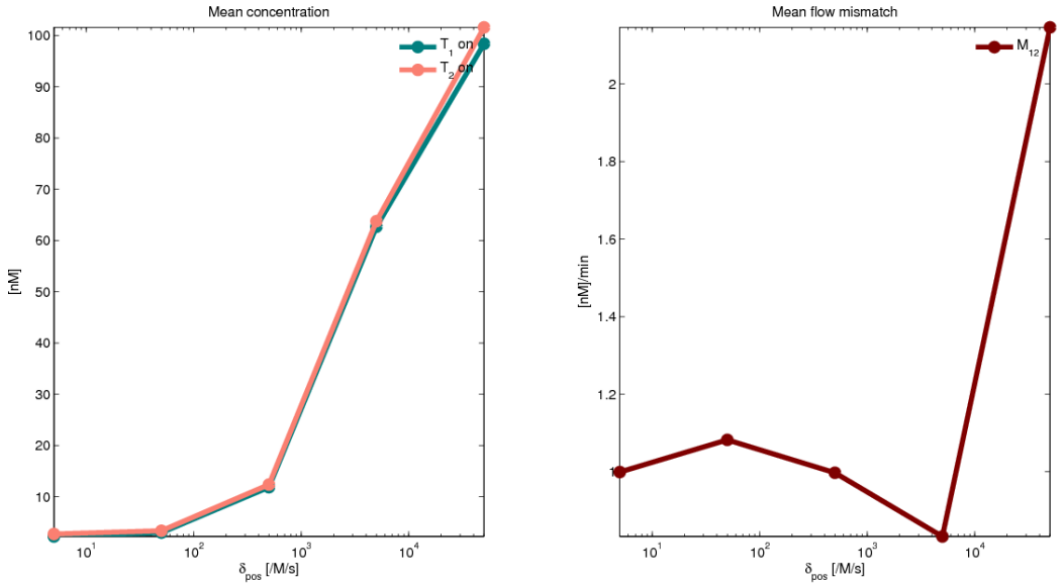

(b)

Figure 21: System with both positive and negative feedback. If $\alpha_{\mathrm{i,pos}} \neq 0$: steady state values of mean concentrations and mean flow mismatches (a) decrease if δ negative increases and (b) tend to increase if δ positive increases.

5 Hill function and mass action kinetics models: a comparison

Consider a single gene T with a "load", i.e. a gene interacting with other molecules that require it to produce a certain amount of R. To regulate the production of R in order to match the load request, it is necessary to insert some feedback loop. A feedback can be described not only by means of mass action chemical reactions, but also with a Hill function model. A Hill function model for negative feedback has been considered and the performances of the different models have been compared. A Hill function model for negative feedback can be obtained starting from these chemical reactions:

$$\begin{aligned}
&\mathrm{T} \xrightarrow{\beta} \mathrm{T} + \mathrm{R} && \text{production,}\\
&\mathrm{T} + \mathrm{nR} \underset{\gamma^-}{\overset{\gamma^+}{\rightleftharpoons}} \mathrm{T}^* && \text{negative feedback,}\\
&\mathrm{R} \xrightarrow{\mathrm{k}} \emptyset && \text{degradation,}\\
&[\mathrm{T}^{\mathrm{tot}}] = [\mathrm{T}] + [\mathrm{T}^*] && \text{constraint.}
\end{aligned}$$

From the ODE

$$\frac{\mathrm{d}[\mathrm{T}^*]}{\mathrm{dt}} = \gamma^+[\mathrm{T}][\mathrm{R}]^{\mathrm{n}} - \gamma^-[\mathrm{T}^*]$$

by means of the Quasi Steady State Approximation (QSSA) we obtain

$$\begin{aligned}
&0 = \gamma^+[\mathrm{T}][\mathrm{R}]^{\mathrm{n}} - \gamma^-([\mathrm{T}^{\mathrm{tot}}] - [\mathrm{T}])\\
&[\bar{\mathrm{T}}] = \frac{\gamma^-[\mathrm{T}^{\mathrm{tot}}]}{\gamma^- + \gamma^+[\mathrm{R}]^{\mathrm{n}}} = [\mathrm{T}^{\mathrm{tot}}]\frac{\Gamma^{\mathrm{n}}}{\Gamma^{\mathrm{n}} + [\mathrm{R}]^{\mathrm{n}}}, \quad \text{where } \Gamma^{\mathrm{n}} = \frac{\gamma^-}{\gamma^+}
\end{aligned}$$

Then, if we substitute $[\bar{\mathrm{T}}]$ in the dynamics of species R, we take into account a consumption term (n molecules of R are used up in the negative feedback reaction) and we consider the degradation as due to the presence of a load U, we achieve

$$\frac{\mathrm{d}[\mathrm{R}]}{\mathrm{dt}} = \beta[\mathrm{T}] - \delta[\mathrm{R}][\mathrm{U}] - \mathrm{n}\gamma^-[\mathrm{R}]^{\mathrm{n}}[\mathrm{T}] = (\beta - \mathrm{n}\gamma^-[\mathrm{R}]^{\mathrm{n}})[\mathrm{T}^{\mathrm{tot}}]\frac{\Gamma^{\mathrm{n}}}{\Gamma^{\mathrm{n}} + [\mathrm{R}]^{\mathrm{n}}} - \delta[\mathrm{R}][\mathrm{U}]$$

The performance of this system can be compared to those of systems with negative feedback, positive feedback and both, modeled with mass action kinetics in presence of the same load U (which, from the point of view of the only gene considered, plays exactly the part of *the other gene* in the simple two gene system). The results of numerical simulation are shown in Fig. 22 and 23. It is possible to see that stoichiometric negative feedback keeps concentrations at a lower level with respect to Hill function negative feedback. While, if we compare the different stoichiometric feedback schemes, we see that with positive feedback concentrations are higher than with negative feedback, and the behavior of the system with both positive and negative feedback ranks somewhere in between.

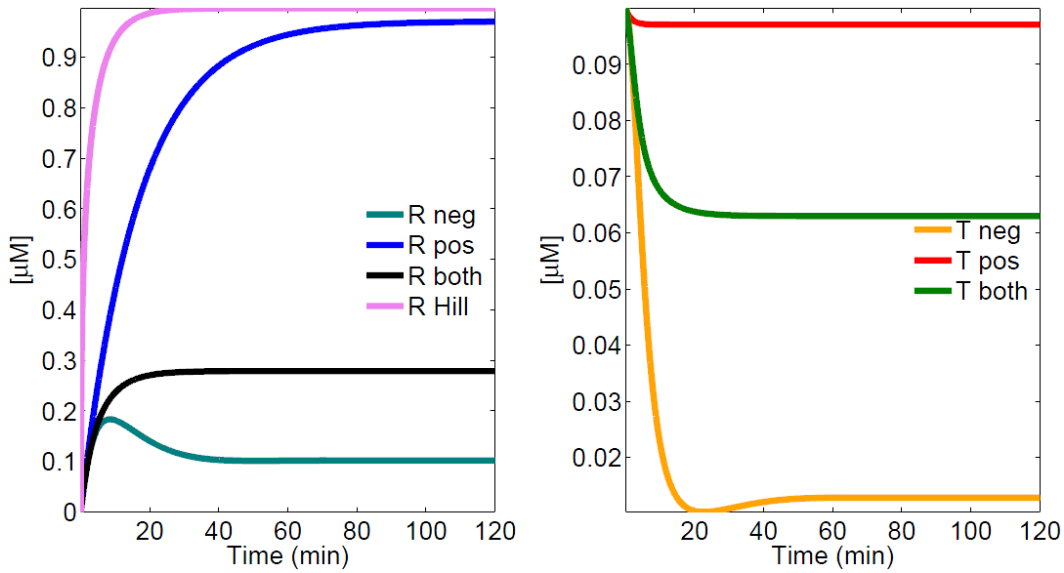

(a)

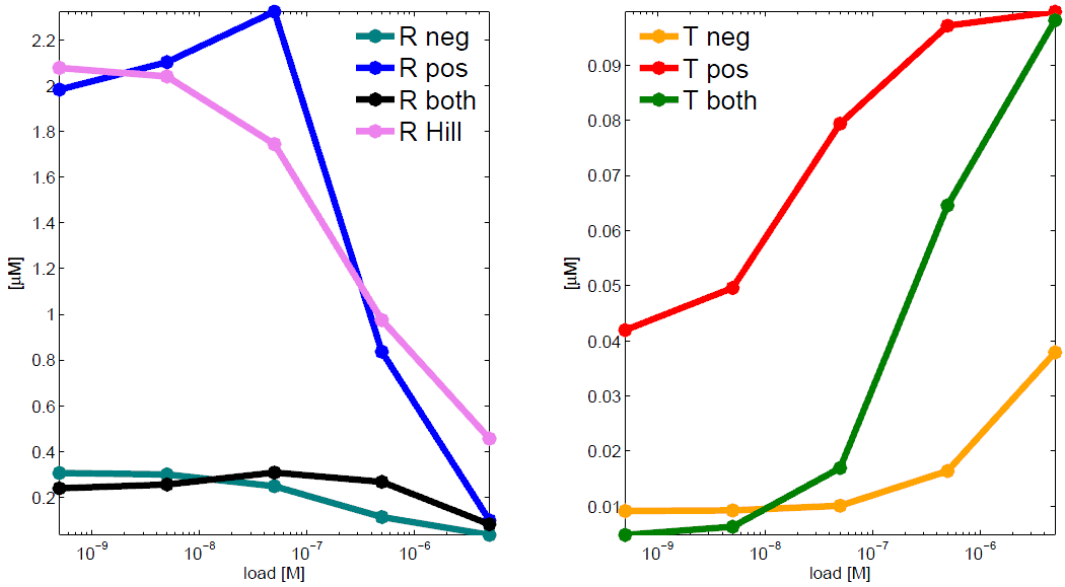

(b)

Figure 22: Single gene with a "load", comparison between different stoichiometric feedbacks and Hill function model for negative feedback: (a) compared numerical ODE solutions; (b) steady state value of concentrations with different loads.

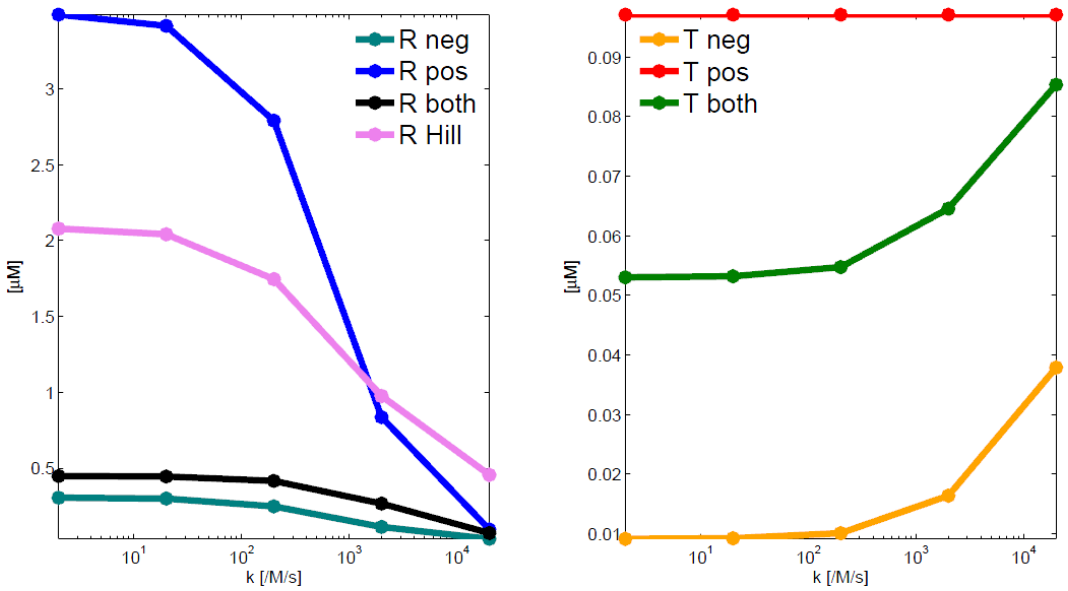

(a)

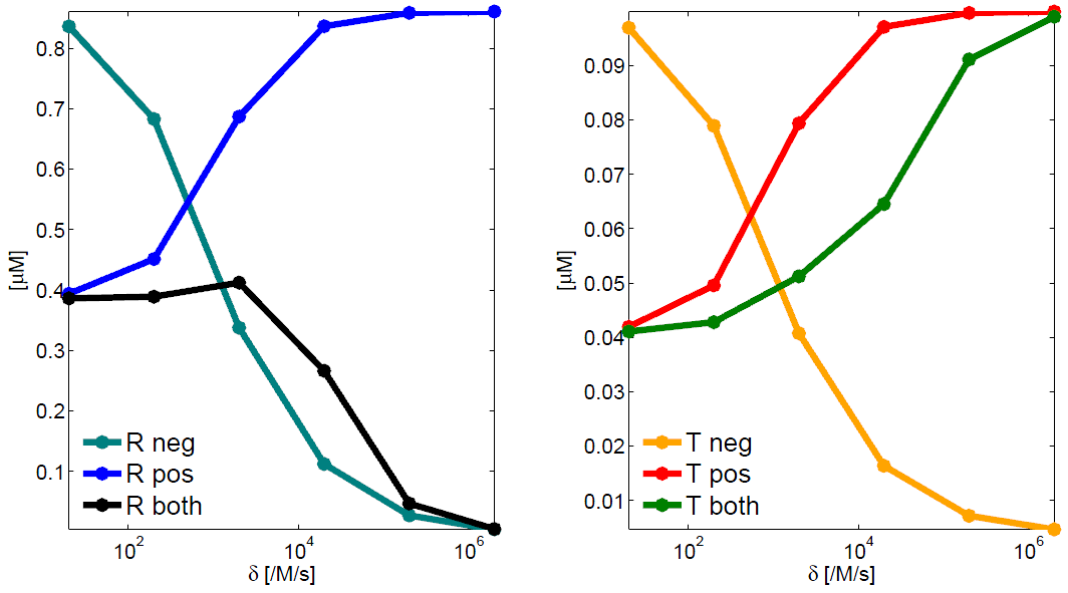

(b)

Figure 23: Single gene with a "load", comparison between different stoichiometric feedbacks and Hill function model for negative feedback: (a) steady state value of concentrations with different values of k; (b) steady state value of concentrations with mass action kinetics models as a function of the feedback strength δ.

6 Negative feedback: a new model for a viable implementation

6.1 A viable DNA strand implementation: domain level design

The negative feedback rate–regulators are the ones we prefer to implement, because of their satisfactory properties and behavior shown by means of numerical simulations. The models considered in 3.2 are simplified and can give us an idea of the biochemical system behavior, but to study a possible experimental implementation, with transcriptional circuits, we need to develop a more complex model, which has to be much more fitting to the biochemical reactions actually occurring. The more accurate model describing the transcriptional circuit implementation of the negative feedback scheme is an extension of the one expounded and derived in [3], which takes into consideration two genes only, but can be adapted to be suitable for a larger number of genes as well. In this case, the "handshake" connection has been considered, because it is the most scalable and the easiest to actually implement with transcriptional circuits. By the way, in the three genes case the "neighbor" and the "handshake" connections coincide.

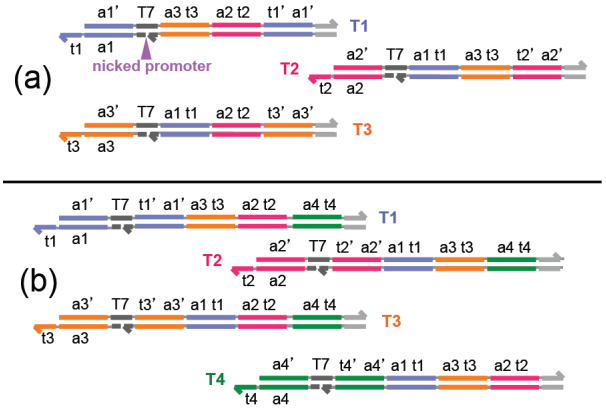

Figure 24: DNA-domain implementation of the (a) three and (b) four genes negative feedback interconnection. Complementary domains have the same color. Nicked T7 promoters are in dark gray, terminator domains in light gray. The RNA output of each genelet is designed to be complementary to its activator strand. RNA species are pairwise complementary.

Previously proposed implementation for two genes

In the two gene system, the transcriptional circuit implementation proposed in [3] consists in two genelets such that the two RNA outputs of each genelet are designed to be complementary to the corresponding activator strand and complementary to each other, so that they can bind to form a product. The two species T_1 and T_2 correspond to two genelet switches, whose RNA transcripts (the output reagents R_1 and R_2) are designed to bind and form a complex P. Once R_1 and R_2 are bound and form P, the complex must be inert and all the regulatory domains for negative auto–regulation (or cross–activation, in general) must be covered, as it is highlighted in Fig. 25.

In the two genes negative feedback case (self–repression), shown in Fig. 26, in addition to the desired self–inhibition loops due to the binding of the two complementary RNA species, an undesired binding between T_i and R_j is introduced. This can be considered as another off state: the complex obtained is a substrate for RNaseH and the RNA strand is degraded by the enzyme, releasing the genelet activation domain. Undesired effects are anyway assumed not to prevail in the system. The

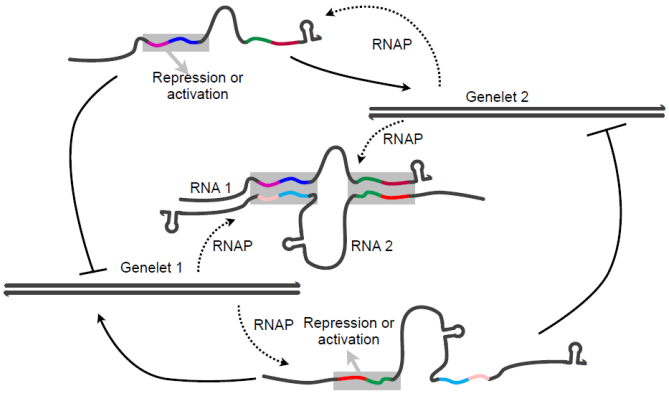

Figure 25: Transcriptional circuit implementation of the two genes interconnection: two RNA species bind to form a product and their regulatory domains are sequestered. When either species is in excess, the feedback loops are active and therefore its regulatory domains are not covered. Figure reproduced from [3].

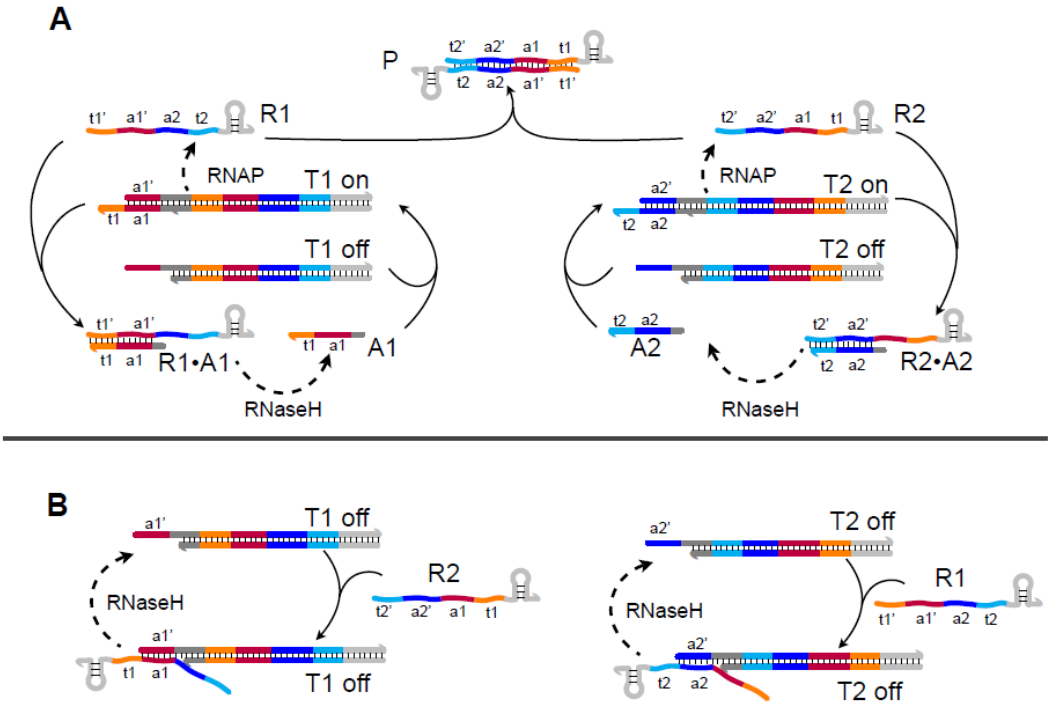

Figure 26: Transcriptional circuit implementation of the two genes negative feedback interconnection: general reaction scheme. Complementary domains have the same color. T7 promoters are in dark gray, terminator hairpin sequences in light gray. The RNA output of each genelet is designed to be complementary to its corresponding activator strand. The two RNA species are also complementary. A) Desired self-inhibition loops. B) Undesired cross–hybridization and RNaseH mediated degradation of the RNA–template complexes. Figures reproduced from [3].

switches T_i and T_j can have three possible states: the on state, in which activator and template are bound and form the complex T_iA_i; the off state given by free T_i; the off state represented by R_j bound to T_i (thus forming T_iR_j). An off state still allows for RNAP weak binding and transcription. The concentration of enzymes is assumed to be considerably lower than that of the DNA molecules, allowing the steady–state assumption for Michaelis–Menten kinetics utilized in the model derivation.

Three and four genes case

The DNA strand implementations proposed for the two genes case can be extended to the case of three or four genes, according for instance to the "neighbor" or the "handshake" scheme (which are anyway completely equivalent in the three genes case). Each genelet needs to be turned on or off depending on the binding of the activator strand and each RNA must be able to bind pairwise with (at least) two of the others to form a product.

Here we describe a possible DNA implementation for our three or four genes handshake negative feedback architecture, with artificial gene networks (transcriptional circuits) [13]. The working principles of these circuits were described in Section 2. Referring to Figure 24, domains of the genes are represented as sequences of bases with different colors. RNA outputs of each gene are not shown, but their domains are identical to the transcribed regions of the genes (downstream of the promoter, dark gray). Domains with the same color are complementary and are expected to bind. The domain annotated as t_1a_1 on T_1, for instance, is an activator strand which can be displaced by the RNA output R_1, which has the domain $t_1'a_1'$. Output RNAs R_i are designed to be complementary to their own activator strands and pairwise complementary to one another, so that they can bind to form products. Once R_i and R_j form P_{ij}, the complex is inert and all the regulatory domains for negative auto–regulation are covered. This design is an extension of that proposed in [17] for a two-gene interconnection. This choice of the domains introduces, in addition to the desired self–inhibition loops, an undesired binding between T_i and R_j. The resulting complex can be considered as another off state of the gene: the complex obtained is a substrate for RNaseH and the RNA strand is degraded by the enzyme, releasing the activating strand.

We built a detailed model of this system, based on the expected domain interactions. Each gene T_i can have three possible states: the on state, in which activator and template are bound and form the complex T_iA_i; the off state given by free T_i; the off state represented by R_j bound to T_i (thus forming T_iR_j). To be sure that the inhibition rate is the same for all the genes, it is better to place the self–inhibition domains $t_i'\,a_i'$ in the same position inside the strand; for example, first (near the $3'$ end) or last (near the $5'$ end) domain (in Figure 24, self-inhibition domains are at the $3'$ end). In the case of more than two genes, when the complex R_iR_j forms, we cannot avoid the formation of loops or torsions for some values of i, j. For example, referring to Figure 24, the R_2 and R_1 complex (binding of the domains indexed 1 and 2) occurs by formation of a loop in the domain a_3t_3 on R_2. It is evident that it is possible to form a complex between R_n and R_m iff, going through one strand in the arrow direction (from 5' to 3') you find at first $t_m'\,a_m'$ and then $a_n\,t_n$, while going through the other strand you find at first $t_n'\,a_n'$ and then $a_m\,t_m$. Placing all the self–inhibition domains $t_i'\,a_i'$ either at the beginning or at the end of the RNA strand assures that this condition is satisfied and thus the binding can successfully occur. So, in the n genes case, there can be $2 \cdot ((n-1)!)^n$ different domain level designs for a DNA strand implementation of the negative feedback architecture for rate–regulation: the self–inhibition domains can be in the first position inside the strand or in the last; in each of these 2 cases, the possible permutations of the other segments are $((n-1)!)^n$ because there are $(n-1)!$ possible different configurations in each of the n strands.

In the three genes case there can be 16 different domain level designs for a DNA strand imple-

mentation of the negative feedback architecture for rate–regulation. The self–inhibition domains can be in the first position inside the strand or in the third; in each of these 2 cases, the possible permutations of the other segments are 8 (2^3, because there are 2 possible different configurations in each of the 3 strands). The possible combinations are shown in Fig. 27 (self–inhibition domains in the first position) and 28 (self–inhibition domains in the first position).

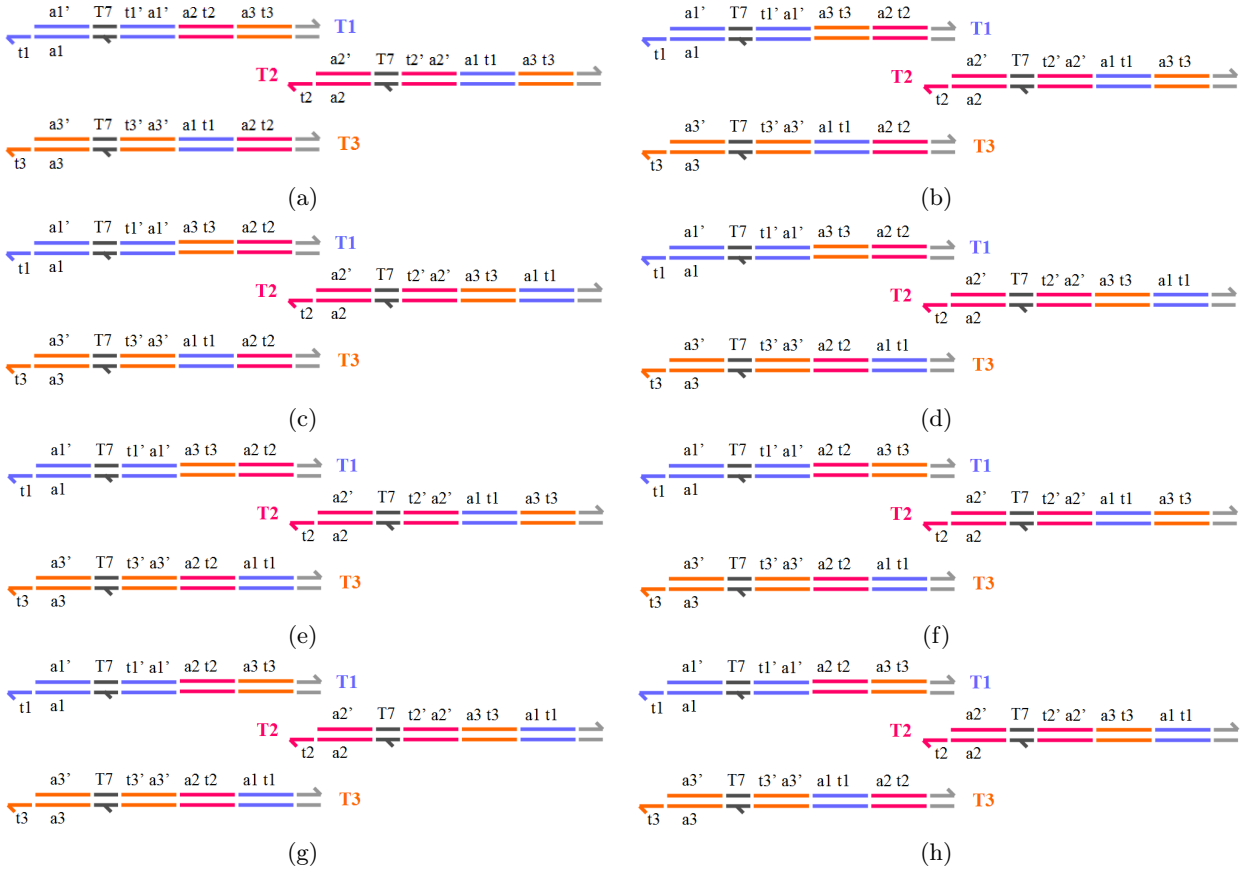

Figure 27: Transcriptional circuit implementation of the three genes negative feedback interconnection: possible domain level designs with the self–inhibition domains in the first position. Complementary domains have the same color. T7 promoters are in dark gray, terminator hairpin sequences in light gray. The RNA output of each genelet is designed to be complementary to its corresponding activator strand. The RNA species are also pairwise complementary.

In the four genes case, instead, the possible different domain level designs for a DNA strand implementation of the negative feedback architecture are 2592. The self–inhibition domains can be in the first position inside the strand or in the fourth; in each of these 2 cases, the possible permutations of the other segments are 1296 (6^4, because there are $3 \cdot 2$ possible different configurations in each of the 4 strands). A couple of the possible combinations are shown in Fig. 29.

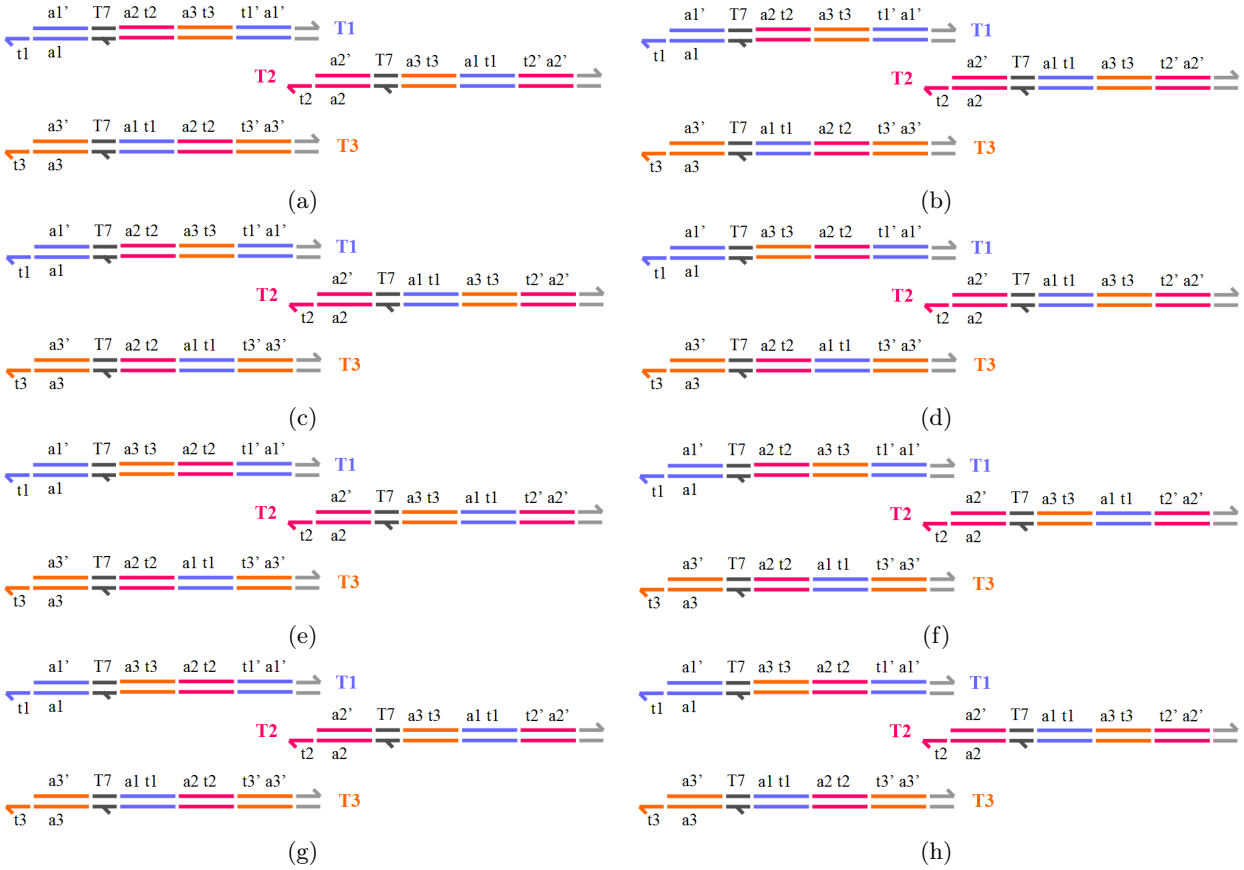

Figure 28: Transcriptional circuit implementation of the three genes negative feedback interconnection: possible domain level designs with the self–inhibition domains in the third position. Complementary domains have the same color. T7 promoters are in dark gray, terminator hairpin sequences in light gray. The RNA output of each genelet is designed to be complementary to its corresponding activator strand. The RNA species are also pairwise complementary.

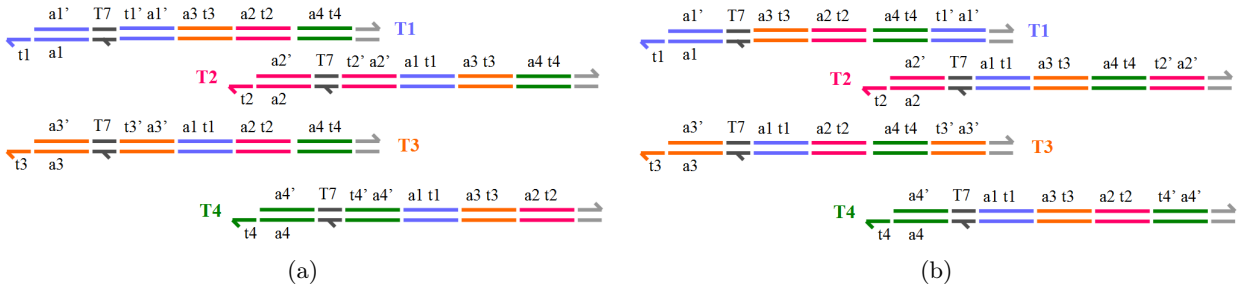

Figure 29: Transcriptional circuit implementation of the four genes negative feedback interconnection: a couple of examples of possible domain level designs. Complementary domains have the same color. T7 promoters are in dark gray, terminator hairpin sequences in light gray. The RNA output of each genelet is designed to be complementary to its corresponding activator strand. The RNA species are also pairwise complementary.

6.2 A more complex model

Including all reactions occurring in the system [17], we can build the following ODEs, where $i = 1, ..., n$,

$$\frac{\mathrm{d}[\mathrm{T_i}]}{\mathrm{dt}} = -\mathrm{k_{T_iA_i}}[\mathrm{T_i}][\mathrm{A_i}] + \mathrm{k_{R_iT_iA_i}}[\mathrm{R_i}][\mathrm{T_i \cdot A_i}] - \mathrm{k_{R_jT_i}}[\mathrm{R_j}][\mathrm{T_i}] + \sum_{\mathrm{j \neq i}} \mathrm{k_{catH_{ji}}}[\mathrm{RNaseH \cdot R_j \cdot T_i}],$$

$$\frac{\mathrm{d}[\mathrm{A_i}]}{\mathrm{dt}} = -\mathrm{k_{T_iA_i}}[\mathrm{T_i}][\mathrm{A_i}] - \mathrm{k_{R_iA_i}}[\mathrm{R_i}][\mathrm{A_i}] + \mathrm{k_{catH_i}}[\mathrm{RNaseH \cdot R_i \cdot A_i}],$$

$$\begin{aligned}\frac{\mathrm{d}[\mathrm{R_i}]}{\mathrm{dt}} = &- \sum_{\mathrm{j \neq i}} \mathrm{k_{R_iR_j}}[\mathrm{R_i}][\mathrm{R_j}] + \mathrm{k_{R_iT_iA_i}}[\mathrm{R_i}][\mathrm{T_i \cdot A_i}] - \mathrm{k_{R_iT_j}}[\mathrm{R_i}][\mathrm{T_j}] - \mathrm{k_{R_iA_i}}[\mathrm{R_i}][\mathrm{A_i}] \\ &+ \mathrm{k_{catONi}}[\mathrm{RNAP \cdot T_i \cdot A_i}] + \mathrm{k_{catOFF_i}}[\mathrm{RNAP \cdot T_i}] + \sum_{\mathrm{j \neq i}} \mathrm{k_{catOFF_{ji}}}[\mathrm{RNAP \cdot R_j \cdot T_i}],\end{aligned}$$

$$\frac{\mathrm{d}[\mathrm{R_i \cdot R_j}]}{\mathrm{dt}} = +\mathrm{k_{R_iR_j}}[\mathrm{R_i}][\mathrm{R_j}],\ \mathrm{j \neq i}$$

$$\frac{\mathrm{d}[\mathrm{R_j \cdot T_i}]}{\mathrm{dt}} = +\mathrm{k_{R_jT_i}}[\mathrm{R_j}][\mathrm{T_i}] - \mathrm{k_{catH_{ji}}}[\mathrm{RNaseH \cdot R_j \cdot T_i}],\ \mathrm{j \neq i}.$$

under proper assumptions we can use Michaelis–Menten quasi–steady–state approximation and substitute these expressions

$$[\mathrm{RNAP \cdot T_i \cdot A_i}] = \frac{[\mathrm{RNAP^{tot}}]\ [\mathrm{T_i \cdot A_i}]}{\mathrm{P \cdot k_{MONi}}}$$

$$[\mathrm{RNAP \cdot R_j \cdot T_i}] = \frac{[\mathrm{RNAP^{tot}}]\ [\mathrm{R_j \cdot T_i}]}{\mathrm{P \cdot k_{MOFFji}}}$$

$$[\mathrm{RNAP \cdot T_i}] = \frac{[\mathrm{RNAP^{tot}}]\ [\mathrm{T_i}]}{\mathrm{P \cdot k_{MOFFi}}}$$

$$[\mathrm{RNaseH \cdot R_i \cdot A_i}] = \frac{[\mathrm{RNaseH^{tot}}]\ [\mathrm{R_i \cdot A_i}]}{\mathrm{H \cdot k_{MHi}}}$$

$$[\mathrm{RNaseH \cdot R_j \cdot T_i}] = \frac{[\mathrm{RNaseH^{tot}}]\ [\mathrm{R_j \cdot T_i}]}{\mathrm{H \cdot k_{MHji}}}$$

where

$$\mathrm{P} = [\mathrm{RNAP^{tot}}]/[\mathrm{RNAP}] = 1 + \sum_{\mathrm{i=1}}^{\mathrm{n}} \frac{[\mathrm{T_i \cdot A_i}]}{\mathrm{k_{MONi}}} + \sum_{\mathrm{i=1}}^{\mathrm{n}} \frac{[\mathrm{T_i}]}{\mathrm{k_{MOFFi}}} + \sum_{\mathrm{j \neq i}} \frac{[\mathrm{R_i \cdot T_j}]}{\mathrm{k_{MOFFij}}}$$

$$\mathrm{H} = [\mathrm{RNaseH^{tot}}]/[\mathrm{RNaseH}] = 1 + \sum_{\mathrm{i=1}}^{\mathrm{n}} \frac{[\mathrm{R_i \cdot A_i}]}{\mathrm{k_{MHi}}} + \sum_{\mathrm{j \neq i}} \frac{[\mathrm{R_i \cdot T_j}]}{\mathrm{k_{MHij}}}$$

The ODEs derived with this new, more complete model have been solved numerically for the cases of three and four genes and the results are shown in Fig. 30. The negative feedback rate–regulation seems thus to work well also when we consider the more complete and accurate model, which can be experimentally implemented and tested by means of transcriptional circuits.

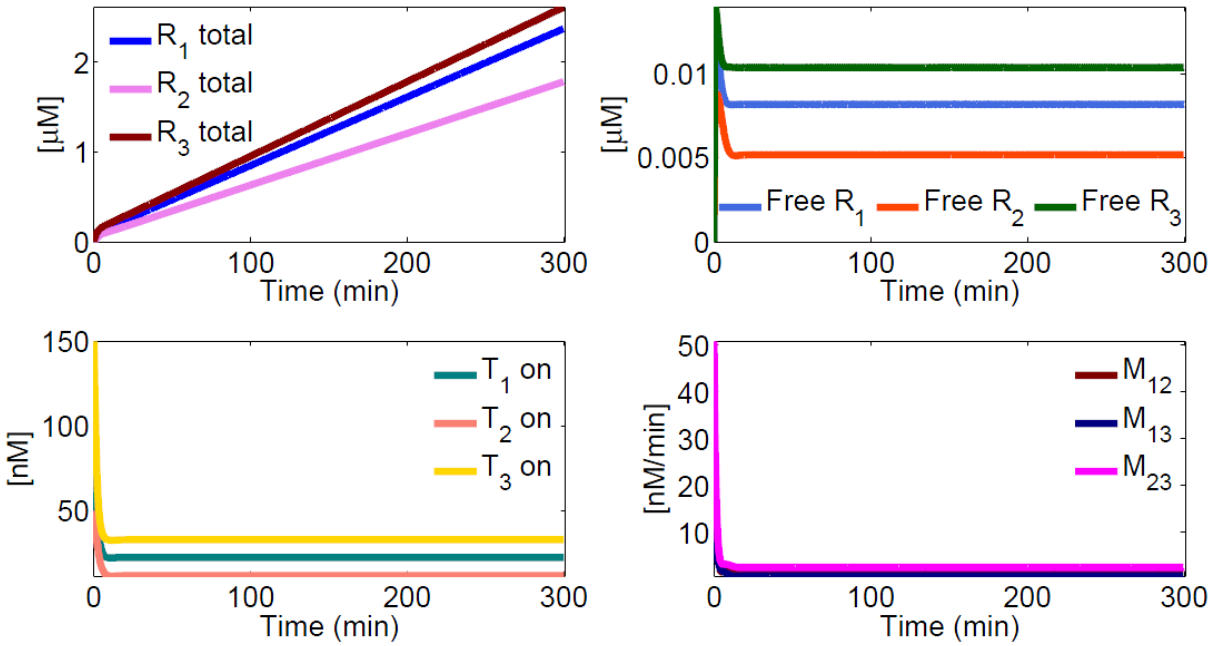

(a)

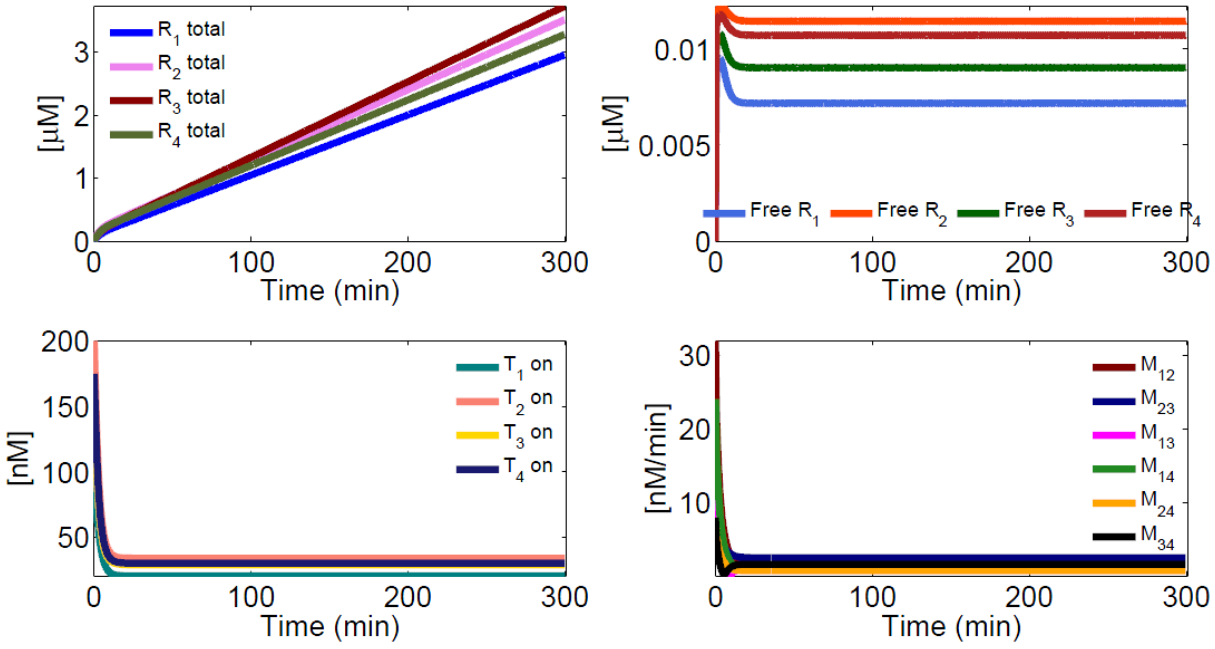

(b)

Figure 30: Transcriptional circuit implementation of the negative feedback scheme: numerical ODE solutions for the case of (a) 3 genes and (b) 4 genes.

7 Results discussion

We considered different feedback architectures to regulate the production of RNA species in a synthetic n–gene system, where these species interact with one another to produce one or more complexes. This problem is relevant in the context of *in vitro* synthetic biology and nanotechnology, where synthetic gene networks are useful as circuits producing components that assemble in nanostructures or that orchestrate dynamic behaviors for molecular computations.

Rate-regulation circuits were scaled up, proposing some theoretical general models for n genes, according to different combinations for product formation, and showing their effectiveness through numerical simulations up to four genes. Feedback loops were designed based on negative feedback (self–inhibition, which can minimize the potentially harmful amount of molecules not used to form the product), positive feedback (cross–activation, which can maximize the overall output flux) and both. Our numerical analysis for $n = 3$ and $n = 4$ revealed that negative autoregulation guarantees better scalability and faster response than positive feedback based architectures. The performances of feedback generated with mass action kinetics and feedback described by Hill functions were compared; both are effective, but stoichiometric negative feedback keeps concentrations at a lower level. After having considered and compared different schemes, since the mass action kinetics negative feedback architecture seems to have the most interesting features and to be the easiest to implement, it was subject to a further investigation. So, for the case of negative feedback, a more accurate model was considered and simulated in the cases of three and four genes. Since the mismatch reduction was still significantly and very fast achieved, a viable DNA strand implementation was devised for this system, for both the networks of three and four genes. Our results provide useful predictions for the future experimental construction of these *in vitro* genetic networks.

Future research goals

The results obtained during the development of this project suggest that the theoretical analysis and the concrete realization *in vitro* of biomolecular rate–regulator circuitry deserve to be continued. Here are some possible targets for future research.

- ***In vitro* realization**: basing on the devised DNA strand implementation, it would be possible to run genelets experiments and actually build *in vitro* one of the circuits considered: comparing the experimental data to simulation results would hopefully validate the ideas and the models produced.

- **Numerical sensitivity analysis of parameters**: to examine the sensitivity to parameter variation and the robustness of the models, Bayesian techniques for parameter space analysis may be useful [14, 20]. It may be possible to fit the parameters of our models, comparing the theoretical system behavior not to actual experimental data, but to fictitious data obtained from the ideal behavior we want the system to show.

- **Consensus and cooperation algorithms** [21]: can they be applied to biochemical systems, to describe rate–regulation systems that involve a growing number of genes? Can we establish a complete formal parallel between rate–regulation biochemical networks and networks based on consensus and cooperation algorithms? It might be interesting to make a further effort in order to exhaustively answer these theoretical questions.

8 Methods: numerical simulations

The various systems were numerically analyzed using scripts expressly written in MATLAB (©The MathWorks). Differential equations were solved using the `ode23` routine. A constant reference for the choice of parameter values was [3].

Here the set of parameter values used to perform the simulation is given for each of the plots shown in the present paper.

Fig. 9 (a) and Fig. 10:

$\alpha_i = 3 \cdot 10^{-4}\, s^{-1}$, $\beta_i = 1 \cdot 10^{-2}\, s^{-1}$, $\delta_i = 5 \cdot 10^{3}\, M^{-1}s^{-1}$ for $i = 1, 2, 3$ and $k_{12} = k_{23} = k_{13} = 2 \cdot 10^{3}\, M^{-1}s^{-1}$. $[\mathrm{T}_1^{\mathrm{tot}}] = 100\,\mathrm{nM}$, $[\mathrm{T}_2^{\mathrm{tot}}] = 200\,\mathrm{nM}$, $[\mathrm{T}_3^{\mathrm{tot}}] = 300\,\mathrm{nM}$.

Fig. 9 (b):

$\alpha_i = 3 \cdot 10^{-4}\, s^{-1}$, $\beta_i = 1 \cdot 10^{-2}\, s^{-1}$, $\delta_i = 5 \cdot 10^{3}\, M^{-1}s^{-1}$ for $i = 1, 2, 3, 4$ and $k_{12} = k_{23} = k_{13} = k_{14} = k_{24} = k_{34} = 2 \cdot 10^{3}\, M^{-1}s^{-1}$. $[\mathrm{T}_1^{\mathrm{tot}}] = 100\,\mathrm{nM}$, $[\mathrm{T}_2^{\mathrm{tot}}] = 200\,\mathrm{nM}$, $[\mathrm{T}_3^{\mathrm{tot}}] = 300\,\mathrm{nM}$, $[\mathrm{T}_4^{\mathrm{tot}}] = 150\,\mathrm{nM}$.

Fig. 11:

$\alpha_i = 3 \cdot 10^{-4}\, s^{-1}$, $\beta_i = 1 \cdot 10^{-2}\, s^{-1}$, $\delta_i = 5 \cdot 10^{3}\, M^{-1}s^{-1}$ for $i = 1, 2, 3, 4$ and $k_{12} = k_{23} = k_{14} = k_{34} = 2 \cdot 10^{3}\, M^{-1}s^{-1}$. $[\mathrm{T}_1^{\mathrm{tot}}] = 100\,\mathrm{nM}$, $[\mathrm{T}_2^{\mathrm{tot}}] = 200\,\mathrm{nM}$, $[\mathrm{T}_3^{\mathrm{tot}}] = 300\,\mathrm{nM}$, $[\mathrm{T}_4^{\mathrm{tot}}] = 150\,\mathrm{nM}$.

Fig. 12:

$\alpha_i = 3 \cdot 10^{-4}\, s^{-1}$, $\beta_i = 1 \cdot 10^{-2}\, s^{-1}$, $\delta_i = 5 \cdot 10^{3}\, M^{-1}s^{-1}$ for $i = 1, 2, 3$ and $k = 6 \cdot 10^{3}\, M^{-1}s^{-1}$. $[\mathrm{T}_1^{\mathrm{tot}}] = 100\,\mathrm{nM}$, $[\mathrm{T}_2^{\mathrm{tot}}] = 200\,\mathrm{nM}$, $[\mathrm{T}_3^{\mathrm{tot}}] = 300\,\mathrm{nM}$.

Fig. 13:

$\alpha_i = 3 \cdot 10^{-4}\, s^{-1}$, $\beta_i = 1 \cdot 10^{-2}\, s^{-1}$, $\delta_i = 5 \cdot 10^{2}\, M^{-1}s^{-1}$ for $i = 1, 2, 3, 4$ and $k = 6 \cdot 10^{3}\, M^{-1}s^{-1}$. $[\mathrm{T}_1^{\mathrm{tot}}] = 100\,\mathrm{nM}$, $[\mathrm{T}_2^{\mathrm{tot}}] = 200\,\mathrm{nM}$, $[\mathrm{T}_3^{\mathrm{tot}}] = 300\,\mathrm{nM}$, $[\mathrm{T}_4^{\mathrm{tot}}] = 150\,\mathrm{nM}$.

Fig. 15:

$\alpha_i = 3 \cdot 10^{-4}\, s^{-1}$ and $\beta_i = 1 \cdot 10^{-2}\, s^{-1}$ for $i = 1, 2, 3$, $\delta_{12} = \delta_{23} = \delta_{13} = \delta_{21} = \delta_{32} = \delta_{31} = 5 \cdot 10^{1}\, M^{-1}s^{-1}$ and $k_{12} = k_{23} = k_{13} = 2 \cdot 10^{3}\, M^{-1}s^{-1}$. $[\mathrm{T}_1^{\mathrm{tot}}] = 100\,\mathrm{nM}$, $[\mathrm{T}_2^{\mathrm{tot}}] = 200\,\mathrm{nM}$, $[\mathrm{T}_3^{\mathrm{tot}}] = 300\,\mathrm{nM}$.

Fig. 16:

$\alpha_i = 3 \cdot 10^{-4}\, s^{-1}$ and $\beta_i = 1 \cdot 10^{-2}\, s^{-1}$, $\delta_i = 5 \cdot 10^{1}\, M^{-1}s^{-1}$ for $i = 1, 2, 3$ and $k = 6 \cdot 10^{3}\, M^{-1}s^{-1}$. $[\mathrm{T}_1^{\mathrm{tot}}] = 100\,\mathrm{nM}$, $[\mathrm{T}_2^{\mathrm{tot}}] = 200\,\mathrm{nM}$, $[\mathrm{T}_3^{\mathrm{tot}}] = 300\,\mathrm{nM}$.

Fig. 18:

$\alpha_{i,neg} = 3 \cdot 10^{-4}\, s^{-1}$, $\alpha_{i,pos} = 0$, $\beta_i = 1 \cdot 10^{-2}\, s^{-1}$ for $i = 1, 2$ and $k = 2 \cdot 10^{3}\, M^{-1}s^{-1}$. $[\mathrm{T}_1^{\mathrm{tot}}] = 100\,\mathrm{nM}$, $[\mathrm{T}_2^{\mathrm{tot}}] = 200\,\mathrm{nM}$; (a): $\delta_{pos} = 5 \cdot 10^{2}\, M^{-1}s^{-1}$ and $\delta_{neg} = 5 \cdot 10^{3}\, M^{-1}s^{-1}$ while (b): $\delta_{pos} = 5 \cdot 10^{3}\, M^{-1}s^{-1}$ and $\delta_{neg} = 5 \cdot 10^{2}\, M^{-1}s^{-1}$.

Fig. 19:

$\alpha_{i,neg} = 3 \cdot 10^{-4}\, s^{-1}$, $\alpha_{i,pos} = 0$, $\beta_i = 1 \cdot 10^{-2}\, s^{-1}$ for $i = 1, 2$ and $k = 2 \cdot 10^{3}\, M^{-1}s^{-1}$. $[\mathrm{T}_1^{\mathrm{tot}}] = 100\,\mathrm{nM}$, $[\mathrm{T}_2^{\mathrm{tot}}] = 200\,\mathrm{nM}$.

Fig. 20:

$\alpha_{i,pos} = 3 \cdot 10^{-4}\, s^{-1}$, $\alpha_{i,neg} = 0$, $\beta_i = 1 \cdot 10^{-2}\, s^{-1}$ for $i = 1, 2$ and $k = 2 \cdot 10^{3}\, M^{-1}s^{-1}$. $[\mathrm{T}_1^{\mathrm{tot}}] = 100\,\mathrm{nM}$, $[\mathrm{T}_2^{\mathrm{tot}}] = 200\,\mathrm{nM}$; (a): $\delta_{pos} = 5 \cdot 10^{2}\, M^{-1}s^{-1}$ and $\delta_{neg} = 5 \cdot 10^{3}\, M^{-1}s^{-1}$ while (b): $\delta_{pos} = 5 \cdot 10^{3}\, M^{-1}s^{-1}$ and $\delta_{neg} = 5 \cdot 10^{2}\, M^{-1}s^{-1}$.

Fig. 21:

$\alpha_{i,pos} = 3 \cdot 10^{-4}\, s^{-1}$, $\alpha_{i,neg} = 0$, $\beta_i = 1 \cdot 10^{-2}\, s^{-1}$ for $i = 1, 2$ and $k = 2 \cdot 10^{3}\, M^{-1}s^{-1}$. $[\mathrm{T}_1^{\mathrm{tot}}] = 100\,\mathrm{nM}$, $[\mathrm{T}_2^{\mathrm{tot}}] = 200\,\mathrm{nM}$.

Fig. 22 and Fig. 23:

positive feedback $\alpha = 3 \cdot 10^{-4}\, s^{-1}$, $\beta = 1 \cdot 10^{-2}\, s^{-1}$, $k = 2 \cdot 10^{3}\, M^{-1}s^{-1}$, $\delta = 2 \cdot 10^{4}\, M^{-1}s^{-1}$, [U] = 0.5 μM, [T^{tot}] = 100 nM; negative feedback $\alpha = 3{\cdot}10^{-4}\, s^{-1}$, $\beta = 1{\cdot}10^{-2}\, s^{-1}$, $k = 2{\cdot}10^{3}\, M^{-1}s^{-1}$, $\delta = 2 \cdot 10^{4}\, M^{-1}s^{-1}$, [U] = 0.5 μM, [T^{tot}] = 100 nM; both feedbacks $\alpha_{pos} = 3 \cdot 10^{-4}\, s^{-1}$, $\alpha_{neg} = 0$, $\beta = 1 \cdot 10^{-2}\, s^{-1}$, $k = 2 \cdot 10^{3}\, M^{-1}s^{-1}$, $\delta_{pos} = \delta_{neg} = 2 \cdot 10^{4}\, M^{-1}s^{-1}$, [U] = 0.5 μM, [T^{tot}] = 100 nM; Hill function $\beta = 1\, s^{-1}$, $\gamma^{-} = 1 \cdot 10^{-2}$, $\Gamma = 0.1 \cdot 10^{-6}$, $n = 2$, $\delta = 2 \cdot 10^{3}\, M^{-1}s^{-1}$, [U] = 0.5 μM, [T^{tot}] = 100 nM.

Fig. 30:

$k_{T_iA_i} = 4 \cdot 10^{4}\, M^{-1}s^{-1}$, $k_{R_iA_i} = 5 \cdot 10^{4}\, M^{-1}s^{-1}$, $k_{R_iT_iA_i} = 5 \cdot 10^{4}\, M^{-1}s^{-1}$, $k_{catON_i} = 6 \cdot 10^{-2}\, s^{-1}$, $k_{catOFF_i} = 1 \cdot 10^{-3}\, s^{-1}$, $k_{catH_i} = 1 \cdot 10^{-1}\, s^{-1}$, $k_{MON_i} = 250 \cdot 10^{-9}\, M$, $k_{MOFF_i} = 1 \cdot 10^{-6}\, M$, $k_{MH_i} = 50{\cdot}10^{-9}\, M$ for $i = 1, ..., n$ and $k_{R_iR_j} = 1{\cdot}10^{6}\, M^{-1}s^{-1}$, $k_{R_iT_j} = 1{\cdot}10^{3}\, M^{-1}s^{-1}$, $k_{MOFF_{ij}} = 1{\cdot}10^{-6}\, M$, $k_{catH_{ij}} = 1 \cdot 10^{-1}\, s^{-1}$, $k_{catOFF_{ij}} = 1 \cdot 10^{-3}\, s^{-1}$, $k_{MH_{ij}} = 50 \cdot 10^{-9}\, M$ for $i = 1, ..., n$, $j \neq i$; (a) $n = 3$, (b) $n = 4$.

Acknowledgments

I would like to thank Richard M. Murray and Elisa Franco for their helpful advise during the development of the project. I also acknowledge financial support by the National Science Foundation (NSF) grant CCF-0832824 (The Molecular Programming Project).

References

[1] S. M. Douglas, I. Bachelet, and G. M. Church, "A logic–gated nanorobot for targeted transport of molecular payloads," *Science*, vol. 335, pp. 831–834, 2012.

[2] K. A. Afonin, E. Bindewald, A. J. Yaghoubian, N. Voss, E. Jacovetty, B. A. Shapiro, and L. Jaeger, "*In vitro* assembly of cubic RNA–based scaffolds designed in silico," *Nature Nanotechnology*, vol. 5, September 2010.

[3] E. Franco, "Analysis, design, and *in vitro* implementation of robust biochemical networks," Ph.D. dissertation, California Institute of Technology, 2011.

[4] U. Alon, *An Introduction to Systems Biology: Design Principles of Biological Circuits.* Chapman & Hall/CRC, 2006.

[5] ——, "Biological networks: The tinkerer as an engineer," *Science*, vol. 301, no. 5641, pp. 1866–1867, 2003.

[6] ——, "Network motifs: theory and experimental approaches," *Nature Reviews Genetics*, vol. 8, no. 6, pp. 450–461, 2007.

[7] F. Blanchini and E. Franco, "Structurally robust biological networks," *Bio Med Central Systems Biology*, vol. 5, no. 1, p. 74, 2011.

[8] E. Franco and R. M. Murray, "Design and performance of *in vitro* transcription rate regulatory circuits," in *Proceedings of the IEEE Conference on Decision and Control*, 2008.

[9] E. Franco, E. Friedrichs, J. Kim, R. Jungmann, R. M. Murray, E. Winfree, and F. C. Simmel, "Timing molecular motion and production with a synthetic transcriptional clock," *Proceedings of the National Academy of Sciences*, vol. 108, no. 40, pp. E784–E793, 2011.

[10] M. B. Elowitz and S. Leibler, "A synthetic oscillatory network of transcriptional regulators," *Nature*, vol. 403, no. 6767, pp. 335–338, 2000.

[11] J. Kim and E. Winfree, "Synthetic *in vitro* transcriptional oscillators," *Molecular Systems Biology*, vol. 7, p. 465, 2011.

[12] C. Sturk, E. Franco, and R. M. Murray, "Tuning a synthetic *in vitro* oscillator using control–theoretic tools," in *Proceedings of the IEEE Conference on Decision and Control*, 2010.

[13] J. Kim, K. S. White, and E. Winfree, "Construction of an *in vitro* bistable circuit from synthetic transcriptional switches," *Molecular Systems Biology*, vol. 2, p. 68, 2006.

[14] P. Subsoontorn, J. Kim, and E. Winfree, "Ensemble bayesian analysis of bistability in a synthetic transcriptional switch," *ACS Synthetic Biology*, 2012.

[15] H. Gu, J. Chao, S.-J. Xiao, and N. C. Seeman, "Dynamic patterning programmed by DNA tiles captured on a DNA origami substrate," *Nature Nanotechnology*, vol. 4, no. 4, pp. 245–248, 2009.

[16] A. Phillips and L. Cardelli, "A programming language for composable DNA circuits," *Journal of The Royal Society Interface*, 2009.

[17] E. Franco, P.-O. Forsberg, and R. M. Murray, "Design, modeling and synthesis of an *in vitro* transcription rate regulatory circuit," in *Proceedings of the American Control Conference*, 2008.

[18] G. Giordano, E. Franco, and R. M. Murray, "Feedback architectures to regulate flux of components in artificial gene networks, *submitted*."

[19] B. Yurke and A. P. Mills, "Using DNA to power nanostructures," *Genetic Programming and Evolvable Machines*, vol. 4, pp. 111–122, 2003.

[20] C. P. Barnes, D. Silk, X. Sheng, and M. P. H. Stumpf, "Bayesian design of synthetic biological systems," *Proc. Natl. Acad. Sci. U.S.A.*, vol. 108, no. 37, pp. 15 190–15 195, 2011.

[21] R. Olfati-Saber, J. A. Fax, and R. M. Murray, "Consensus and cooperation in networked multi–agent systems," in *Proceedings of the IEEE*, vol. 95, no. 1, January 2007.